Fall 2017

# Optimization of solvent suppression sequences for NMR analysis of aqueous solutions

Annalise Rose Pfaff



Department: Chemistry

# OPTIMIZATION OF SOLVENT SUPPRESSION SEQUENCES FOR NMR ANALYSIS OF AQUEOUS SOLUTIONS

by

ANNALISE ROSE PFAFF

A DISSERTATION

Presented to the Faculty of the Graduate School of the

MISSOURI UNIVERSITY OF SCIENCE AND TECHNOLOGY

In Partial Fulfillment of the Requirements for the Degree

DOCTOR OF PHILOSOPHY

in

CHEMISTRY

2017

Approved by:

Klaus Woelk, Advisor
Nuran Ercal
Jeffrey Winiarz
Daniel Hier
John Hogan

## PUBLICATION DISSERTATION OPTION

This dissertation consists of the following three articles, which have been published or submitted for publication as follows:

Paper I (Pages 13-31): "EXponentially Converging Eradication Pulse Train (EXCEPT) for solvent signal suppression in investigations with variable $T_1$ times," by Emmalou T. Satterfield, Annalise R. Pfaff, Wenjia Zhang, Lingyu Chi, Rex E. Gerald II, and Klaus Woelk has been published in the *Journal of Magnetic Resonance*.

Paper II (Pages 32-49): "Predicting the effect of relaxation during frequency-selective adiabatic pulses," by Annalise Pfaff, Cailyn McKee, and Klaus Woelk has been published in the *Journal of Magnetic Resonance*.

Paper III (pages 50-70): "A fast and convenient way to predict relaxation during a frequency-selective adiabatic hyperbolic secant pulse (HS1 sech pulse)," by Annalise Pfaff and Klaus Woelk has been submitted to the *Journal of Magnetic Resonance.*

## ABSTRACT

When the use of deuterated solvents is precluded in the NMR analysis of biomolecules in their natural environment, pre-saturation solvent suppression pulse sequences are frequently employed to avoid interference from the overbearing solvent signal. However, these sequences generally require extensive re-adjustment of NMR parameters between samples. For this reason, the EXCEPT (EXponentially Converging Eradication Pulse Train) solvent suppression sequence was developed, which exhibits a tolerance of over an order of magnitude in sample $T_1$ variation. EXCEPT uses an innovative version of "inversion-recovery nulling" with frequency-selective, low-power adiabatic pulses and exponentially decreasing interpulse delays that effectively reduce solvent net magnetization by more than 99.9%. Low-power adiabatic pulses confer stable inversion despite $B_1$-inhomogeneities but are significantly longer than a standard inversion pulse. Differences between experimentally achieved suppressions and those predicted by computer simulations prompted examination of the adiabatic pulse as a source of the discrepancy. These investigations led to the development of a numerical model for predicting relaxation during frequency-selective adiabatic HS1 pulses. The utility of this model is demonstrated for a range of experimental conditions including a wide variation in sample $T_1$ relaxation time, RF pulse power level dampening, and most importantly, when initial net magnetization is not at thermodynamic equilibrium. Investigations of adiabatic HS1 pulses applied to non-equilibrium magnetization revealed a linear relationship between the magnitude of the magnetization before and after the HS1 pulse. The linear relationship facilitates simple and convenient implementation and optimization of NMR sequences in which adiabatic HS1 pulses are employed.

# ACKNOWLEDGMENTS

I would first like to express my deepest gratitude to my parents, Steven and Linda, and my sister, Alyssa. Their unconditional love has supported me throughout my life and allowed me to pursue my goals. They were the first people in my life to instill the curiosity and love of learning that led me to the Chemistry PhD program at Missouri S&T.

Next, I would like to thank my advisor, Dr. Klaus Woelk—under his mentorship, I discovered academic research. I learned to engage difficult problems from a scientific perspective and to value hard-won understanding. I will never forget his encouragement and guidance throughout my years at Missouri S&T. Dr. Ercal has also been a great source of inspiration to me. I will always be grateful for her welcoming my exploration of biochemistry research and the opportunity to work closely with her for several years, and I continue to admire her energy, generosity, and wealth of knowledge. I have been fortunate enough to work with Dr. Winiarz and Dr. Hier in an educational capacity, helping coordinate the general chemistry lab and a neurochemistry course. Dr. Hogan's support and perspective from another field are greatly appreciated as well. The experience and advice given by Drs. Winiarz, Hier, and Hogan are invaluable to me, and I thank them for all they have done on my behalf. I would also like to acknowledge my fellow research group members for their inspiration and support: Emmalou Schmittzehe, Lingyu Chi, Ming Huang, and Cailyn McKee. My colleagues, Sharen Wang and Justin Beltz, have also contributed immensely to my personal and professional development. Finally, as a recipient of the Chancellor's Fellowship, I would like to thank the Missouri S&T Office of Graduate Studies for their generous financial support.

# TABLE OF CONTENTS

# LIST OF ILLUSTRATIONS

SECTION Page

PAPER III

# LIST OF TABLES

# 1. INTRODUCTION

## 1.1. SOLVENT SUPPRESSION FOR NMR ANALYSIS OF AQUEOUS SOLUTIONS

NMR (nuclear magnetic resonance) spectroscopy can accomplish non-destructive, non-invasive one-shot spectroscopic identification and quantification in reaction mixtures. As such, it served as an ideal analytic tool for investigations of hydrothermal biomass-to-fuel (HT-BTF) reactions.(1) For these reactions, cellulosic biomass or model substrates such as glucose are converted to the biofuel precursor 5-HMF (5-hydroxymethylfurfural) and other byproducts at elevated temperatures and pressures.(2, 3) Generally, these reactions are conducted in solution, with analyte concentrations of < 0.1 M. If the solvent is water, the reaction mixture is approximately 110 M in hydrogen atoms (pure water is 55 M). Generally, in a single-pulse $^{1}H$ NMR spectrum, the area under a signal is proportional to the number of hydrogen nuclei resonating at that frequency. Hence, for typical BTF reaction samples, the analyte signals are at least 1000 times smaller than the solvent signal, and therefore one cannot take full advantage of the dynamic range of the spectrometer's analog-to-digital converter (ADC), if the analyte signals can be resolved at all. The solvent signal is also broad, and may additionally interfere with nearby signals via radiation damping or off-resonance effects.(4)

To avoid these issues, deuterated solvents (such as heavy water, $D_2O$) may be substituted for proteo-solvents. Although deuterons have a nonzero nuclear spin ($I = 1$), they possess a very different gyromagnetic ratio ($\gamma$) and therefore precess at a much lower frequency (about 1/6 of the resonance frequency of $^{1}H$ nuclei, leading to approximately 32 MHz for D (= $^{2}H$) compared to 200 MHz for $^{1}H$ at 4.7 T), consequently making them

"invisible" in a typical $^{1}H$ NMR spectrum. However, for reactions conducted in deuterated solvents, other concerns arise. Particularly with the HT-BTF samples, water is often a significant product during the first step of the reaction (formation of 5-HMF), so using a deuterated solvent is unlikely to eliminate a relatively large water signal from the spectrum. The most troublesome issue, however, is that of deuteron-proton exchange between the analytes and solvent (see Figure 1.1) at the elevated temperatures of hydrothermal degradation during both the formation of 5-HMF and its hydrolysis products.(5) This phenomenon was a major impediment to the accurate quantitation of the reaction intermediate 5-HMF, and needed to be avoided by utilizing the native solvent, water.

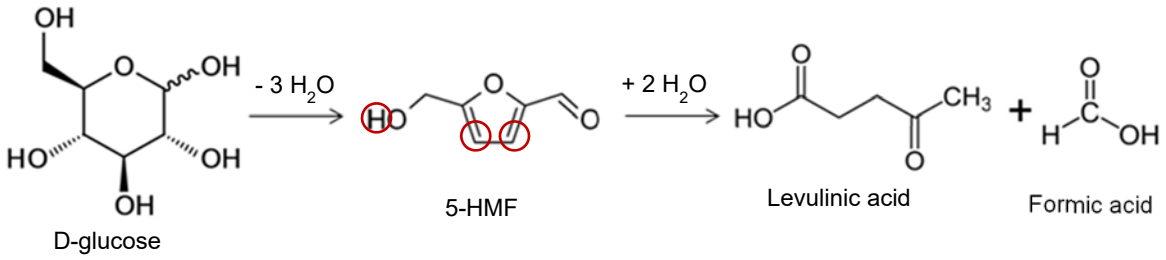


Figure 1.1. Hydrothermal biomass-to-fuel reaction. Exchangeable protons on the product of interest (5-HMF) are circled in red.

Running the reaction in water compelled our research group to address the overwhelming water signal with a solvent suppression sequence. A solvent suppression sequence generally comprises an RF pulse or series of pulses that either destroy the net magnetization or leave it intact but preclude its observation during acquisition. However,

the utility of a given sequence is highly dependent on the nature of the sample and analytes.(6, 7) For the HT-BTF reactions, additives such as mineral acids and metal salts were incorporated to enhance the yield of 5-HMF and/or decrease the formation of byproducts. However, these can alter the microscopic magnetic environment within the sample, thereby changing the relaxation behavior of the nuclei and impacting the performance of the sequence.

## 1.2. RELAXATION AND SOLVENT SUPPRESSION FOR SMALL MOLECULES IN NON-VISCOUS SOLUTIONS

Relaxation is the process by which excited spins return to their thermodynamic equilibrium energy state populations as predicted by the Boltzmann equation. In small-molecule solution NMR, two primary relaxation types are of interest: longitudinal and transverse relaxation. Longitudinal, or spin-lattice, relaxation refers to recovery of net magnetization along the $+z$ axis of the static magnetic field $B_0$, accomplished by the transfer of energy to the surrounding "lattice," which in this case comprises other nuclei in the local environment (enthalpy relaxation). Transverse relaxation, on the other hand, is the loss of net magnetization in the $xy$ plane due to a loss of coherence, or phase alignment of the precessing spins (entropy relaxation). The time constants ascribed to these two processes are $T_1$ and $T_2$, respectively. For fast-tumbling small molecules in non-viscous environments in the extreme-narrowing limit of high $B_0$ fields, these time constants are essentially equal. Because the primary goal of a solvent suppression sequence is to avoid measurement of the solvent net magnetization, the rate at which it recovers after perturbation from equilibrium is crucial to the timing of solvent suppression sequence elements. Continuous-wave saturation, WATERGATE (8), and WET(9) are examples of popular water suppression sequences that were explored and

tested for the analysis of the HT-BTF samples. However, all were too sensitive to changes in the nuclear spin relaxation of the water protons in the samples to accomplish effective suppression without extensive re-adjustment before each analysis.

## 1.3. EXCEPT, A CONVENIENT $T_1$- AND $B_1$-INSENSITIVE SOLVENT SUPPRESSION SEQUENCE

In order to perform NMR analysis of HT-BTF samples in their native solvent (water) without extensive re-adjustment between samples, a new solvent suppression sequence was developed and named EXCEPT (EXponentially Converging Eradication Pulse Train). Using the concept of inversion-recovery nulling, EXCEPT eliminates solvent net magnetization before acquisition of a spectrum. When applied, this sequence inverts net solvent magnetization and allows it to partially recover before inverting it again. (See Paper I Figure 1). This cycle is repeated until the net solvent magnetization is eliminated, at which time a standard 90° excitation pulse is applied and a spectrum is acquired, without the overwhelming solvent signal. The key innovation of EXCEPT was the optimization of the equation governing the length of the delays during which the net magnetization partially recovers, thus achieving reliable suppression over an order of magnitude in $T_1$ variation between samples. This range can also be easily adjusted by modifying a constant factor in the equation used to calculate the delays. Another important component of EXCEPT is the use of frequency-selective adiabatic inversion pulses, which reliably invert the solvent net magnetization over a limited but adjustable range of RF frequencies. With the adjustable range set to the resonance of the water protons, only the water signal is affected by the EXCEPT sequence, while analyte signals remain unperturbed. The pulsed RF field $B_1$ of an NMR spectrometer is responsible for "tipping" the net magnetization by a desired pulse nutation angle (usually 90° for

observation or 180° for inversion of magnetization). For standard pulses, $B_1$ inhomogeneities due to sample variations, instrumental fluctuations, etc. will result in hard-to-predict perturbation of the net magnetization. This is highly undesirable for a solvent suppression sequence that depends on reliable inversion for optimal performance. In contrast, inversion by the adiabatic pulse is largely independent of $B_1$ inhomogeneities. As a result, necessary user adjustments to the sequence between samples should be kept to a minimum, and the solvent signal should be reduced by over 99.9%. With pure water being 110 M in hydrogen nuclei, a water NMR signal that is suppressed 99.9% will still be about as strong as an 0.1 M analyte NMR signal. The EXCEPT sequence that was developed in collaboration with Emmalou Schmittzehe (Satterfield) successfully addresses both issues, variations in nuclear spin relaxation time as well as variations in spectrometer $B_1$ field.

### 1.4. ADIABATIC PULSES

Adiabatic pulses are amplitude- and frequency-modulated NMR pulses designed to achieve stable excitation or inversion of magnetization above a given threshold RF power level.(10) “Adiabatic” refers to the adiabatic theorem of quantum mechanics, which posits that a quantum mechanical system can adapt to sufficiently gradual changes.(11) In the case of adiabatic NMR pulses the net sample magnetization ($M$) follows an effective field ($B_{\text{eff}}$) if it continuously changes the angle $\alpha(t)$ with the main magnetic field $B_0$ until the pulse is terminated. Hence, an adiabatic 90° pulse will move magnetization from the longitudinal axis (+$z$ axis) into the transverse plane ($xy$ plane), while an adiabatic inversion will move it from the +$z$ to the –$z$ axis. A sample

magnetization $M$ will follow $B_{\text{eff}}$ as long as its motion is less than the precession frequency associated with the effective field. This is called the "adiabatic condition." (12)

$$|\omega_{\text{eff}}(t)| \gg |\mathrm{d}\alpha/\mathrm{d}t| \quad (1)$$

During an adiabatic NMR pulse its frequency gradually sweeps over a range centered about $\omega_{\text{LF}}$, the Larmor frequency of the spins of interest. If viewed in a frame of reference rotating at $\omega_{\text{LF}}$, this frequency sweep results in a continuously changing additional field along the $z$ axis ($\Delta B_0$) proportional to the value of the frequency modulation function at time $t$, i.e., $\Delta\omega_0(t)$. The frequency sweep is executed with an RF amplitude (i.e., $B_1$ amplitude) that gradually increases, reaches a maximum, and then decreases. The amplitudes of $B_1$ and $\Delta B_0$, which are the components of $B_{\text{eff}}$, are designed such that $B_{\text{eff}}$ starts out collinear with the $+z$ axis and then gradually changes the angle $\alpha(t)$ towards the $xy$ plane (for excitation pulses) or the $-z$ axis (for inversion pulses).(13)

$$\gamma B_{eff}(t) = \omega_{eff}(t) = \sqrt{\omega_1(t)^2 + \Delta\omega_0(t)^2} \quad (2)$$

$$\alpha(t) = \tan^{-1}\left(\frac{\omega_1(t)}{\Delta\omega_0(t)}\right) = \tan^{-1}\left(\frac{B_1(t)}{\Delta B_0(t)}\right) \quad (3)$$

One of the most popular adiabatic inversion pulses is the hyperbolic secant (HS1) pulse, which was also used in the EXCEPT sequence. The modulation functions for the HS1 pulse are as follows:

Amplitude $$\omega_1(t) = \omega_{1,max}\,\mathrm{sech}\left[\beta\left(\frac{2t}{T_p} - 1\right)\right] \quad (4)$$

Frequency $$\Delta\omega_0(t) = A\tanh\left[\beta\left(\frac{2t}{T_p} - 1\right)\right] \quad (5)$$

where $\omega_1(t)$ is the frequency related to the amplitude of $B_1$ at time $t$, $\omega_{1,\text{max}}(t)$ is the frequency at the maximum $B_1$ amplitude, β is a truncation factor, and $T_\text{p}$ is the pulse width (pulse duration). $A$ is the amplitude of the frequency sweep, and $\Delta\omega_0 = \omega_{\text{RF}}(t) -$

$\omega_{LF}$, where $\omega_{RF}$ is the frequency of $B_1$ at time *t,* and $\omega_{LF}$ is the center frequency of the pulse bandwidth.(14) If the duration of the adiabatic pulse can be made long enough, it allows for the inversion of an arbitrarily narrow range of frequencies (useful when targeting a solvent signal while leaving others untouched) above quite low $B_1$ threshold power levels (easily met even in the presence of sample variation).

Other adiabatic pulses are governed by different modulation functions, but all are designed to excite or invert magnetization within the range of the frequency sweep as long as the adiabatic condition is satisfied. The HS1 pulse was chosen for the EXCEPT sequence not only because of its ability to invert water magnetization without pulse power optimization, but also because it produces a smooth transition at the edges of the bandwidth for EXCEPT suppression in the resulting spectrum and minimizes artifacts observed with the use of other shaped pulses (such as a *sinc* pulse).

## 1.5. ADIABATIC FAST-PASSAGE AND OTHER RELAXATION PROCESSES

A variation of the adiabatic NMR pulse known as adiabatic "fast passage" may be used in place of a conventional "hard" pulse to excite all frequencies in an entire spectral range of interest (i.e., RF bandwidth in the kHz range). For a pulse of a given duration, this requires much stronger $B_1$ fields than utilized for frequency-selective adiabatic pulses in order to stay within the bounds of the adiabatic condition. These pulses are also much shorter (a few milliseconds) than frequency-selective adiabatic pulses, especially when used in highly time-sensitive applications such as *in vivo* imaging. The relatively high $B_1$ fields (with $\omega_{1,max}/2\pi$ of several kHz versus 20 Hz for the HS1 pulse in the EXCEPT sequence) and the nature of the samples for which they are applied necessitate the consideration of other relaxation processes besides standard spin-lattice and spin-spin.

Dipolar interactions are a primary relaxation mechanism for large molecules and viscous samples (e.g., biomacromolecules and tissue samples). If a simple two-spin system is considered, four possible energy levels exist arising from the two possible spin states for each of the two nuclei (α denotes parallel alignment with $B_0$ and β antiparallel alignment): $\alpha_1\alpha_2 < \alpha_1\beta_2 \approx \beta_1\alpha_2 < \beta_1\beta_2$. Cross-relaxation is the process by which the transitions $\alpha_1\alpha_2 \rightarrow \beta_1\beta_2$ ($w_2$ or double-quantum transition) and $\alpha_1\beta_2 \rightarrow \beta_1\alpha_2$ ($w_0$ or zero-quantum transition) contribute to the return to thermodynamic equilibrium energy state populations. Both $w_2$ and $w_0$ occur through dipole-dipole interactions between the two nuclei; however, rapid tumbling such as in small molecules in non-viscous solutions renders dipolar interactions less effective. Dipolar relaxation may also be induced by the strong $B_1$ field required for the adiabatic fast passage used in other types of NMR spectroscopy. Furthermore, chemical exchange, or the transfer of nuclei between different chemical environments, may also result in added relaxation pathways, i.e., relaxation via interaction of excited spins with their new surroundings. Relaxation because of chemical exchange, however, does not contribute significantly under the conditions for which EXCEPT was designed.

The model presented here proposes to predict relaxation during frequency-selective, i.e., long, low-power adiabatic pulses, where the pulse width is on the order of the sample spin-lattice and spin-spin relaxation times, dipolar interactions are ineffective due to the fast-tumbling of small molecules in low-viscosity environments, and chemical exchange does not contribute significantly to relaxation. The method for predicting relaxation during adiabatic pulses introduced in this dissertation should not be misconstrued as an alternative or replacement of that set forth by Sorce *et. al* (14) Mangia

*et al.* (15), and Michaeli *et al.* (16, 17) which applies rotating-frame relaxation for adiabatic pulses with durations of a few milliseconds and strong $B_1$-fields with $\omega_1$ frequencies on the order of kHz in samples where dipolar interactions or chemical exchange are the primary relaxation processes.

## 1.6. RELAXATION DURING FREQUENCY-SELECTIVE ADIABATIC PULSES

While EXCEPT greatly reduces solvent signals despite sample variations that would prove troublesome for other suppression sequences, it was apparent that optimal suppression was still not achieved. The simulations of the observed net magnetization after each inversion and partial recovery cycle that were employed for the optimization of the delay equation (See Section II Figure 2) indicated the solvent signal could theoretically be reduced by at least a factor of 10,000 after 16 cycles. Clearly, the simulation did not account for something that was occurring in the real-life implementation of EXCEPT. The most likely process that was neglected in the simulations was relaxation during the rather long frequency-selective HS1 inversion pulse. On the 200 MHz Bruker AVANCE DRX spectrometer used in these investigations, a conventional "hard" inversion pulse lasts 23 μs. By comparison, the HS1 pulse used for the EXCEPT sequence is 500 ms long, achieving a narrow bandwidth of 60 Hz around the incident HS1 pulse frequency. Normally, relaxation is not considered in the theoretical treatments of short "hard" pulses because the longitudinal and transverse relaxation times of small-molecule analytes in non-viscous solutions (as in HT-BTF samples) are orders of magnitude longer. However, the duration of the HS1 pulse is on the order of the $T_1$ and $T_2$ relaxation times of water in the HT-BTF samples, and the HS1 pulse lasts longer than the last several delays in the EXCEPT sequence. Particularly when

combined with short delays, the long durations of the adiabatic pulses may significantly obstruct the desired effect of inversion-recovery nulling.

The prospect of relaxation during long, low-power adiabatic pulses warranted further investigation as the primary source of discrepancy between experimental and simulated EXCEPT performance. Accurate prediction of net magnetization is important because the optimization algorithm for the delays minimizes net magnetization after the final inversion-recovery cycle. Hence, developing a convenient predictive model for relaxation during the HS1 adiabatic pulse would be instrumental in further optimization of the EXCEPT sequence and better alignment of experimental and simulated suppression.

While relaxation during adiabatic fast passage (i.e., short, high-power, non-frequency selective pulses) has been addressed in the literature (14-17), a convenient method for prediction of frequency-selective adiabatic pulse relaxation conducive to incorporation into computer optimizations was still lacking. The publication entitled "Predicting the effect of relaxation during frequency-selective adiabatic pulses" details the development and validation of such a model. Experimental measurement of net magnetization components at regular intervals during the pulse confirmed that deviation from constant angular motion during the frequency selective HS1 pulse is governed, in part, by the $B_1$ power level dampening. The non-weighted least squares analysis of experimentally measured $\alpha(t)$ as a function of pulse duration ($t$) resulted in a correction factor ($f_{bf}$) to the equation for angular motion of net magnetization with respect to the $+z$ axis:

$$\alpha(t) = \tan^{-1}\left(f_{\mathrm{bf}} \times \frac{B_1(t)}{\Delta B_0(t)}\right). \qquad (6)$$

With this more representative equation for adiabatic angular motion, a stepwise, recursive, parametric solution to the Bloch equations was used to simulate the evolution and relaxation of net magnetization during of the pulse. It is shown that this method offers a reasonably close approximation when compared to experimentally measured magnetization during the HS1 pulse for samples of various relaxation times. Furthermore, both simulated and experimental data indicate relaxation toward thermodynamic equilibrium during the pulse. This is contrasted with descriptions of relaxation during adiabatic fast passages, wherein the responsible processes for relaxation are dipolar interactions and chemical exchange, and where both net magnetization components relax towards zero in the $B_{\text{eff}}$ frame. (14, 17) These mechanisms are not significant under the experimental conditions for which the HS1 pulse in EXCEPT was intended (small-molecule, non-viscous solutions, and low pulse power levels).

This method demonstrates that angular motion and magnitude of net magnetization during frequency-selective adiabatic pulses can be predicted via a convenient numerical model. However, further exploration of its capabilities was warranted, which is described in the manuscript "A fast and simple way to predict relaxation during a frequency-selective adiabatic hyperbolic secant pulse (HS1 sech pulse)." It was particularly necessary to establish validity of the model for initial net magnetizations not at thermodynamic equilibrium because only the first of the many HS1 pulses in the EXCEPT sequence is generally applied to magnetization at thermodynamic equilibrium. More specifically, net magnetization that is not completely recovered from perturbation before the application of an adiabatic pulse, as is the case during the execution of EXCEPT, also needed to be covered by the model introduced in this work.

Simulations using the model described above revealed that, for a given relaxation time, the net magnetization after adiabatic HS1 inversion was directly proportional to the initial magnetization before the execution of the HS1 inversion. This relationship was examined experimentally at different pulse power dampening levels and for samples with varying relaxation times. While the net magnetization after the pulse deviates slightly from that predicted by the simulation, it nevertheless exhibits a linear relationship to the net magnetization before the pulse. Investigating the effects of sample relaxation time and pulse power dampening level was important for extension of the model to other applications of adiabatic pulses. It was shown that the model successfully predicted final net magnetization despite significant changes to pulse power levels through incorporation of the refinement factor derived from the best-fit analysis. The model was similarly robust with respect to variation in sample relaxation time. Finally, the highly predictable relationship between net magnetization before and after frequency-selective adiabatic pulses lends itself to facile implementation of these pulses and optimization of sequences in which they are used.

In summary, the work described in this dissertation addresses the development of solvent suppression sequences and a convenient predictive tool for the optimization thereof. It contributes to the understanding of net magnetization behavior during adiabatic pulses, which find wide usage in magnetic resonance applications such as *in vivo* imaging. It is expected that this work will enable further exploration and innovation in solvent suppression for NMR analysis of biomolecules and tissue samples in their native solvent environment.

# PAPER

# I. EXPONENTIALLY CONVERGING ERADICATION PULSE TRAIN (EXCEPT) FOR SOLVENT-SIGNAL SUPPRESSION IN INVESTIGATIONS WITH VARIABLE $T_1$ TIMES

## ABSTRACT

Selective presaturation is a common technique for suppressing excessive solvent signals during proton NMR analysis of dilute samples in protic solvents. When the solvent $T_1$ relaxation time constant varies within a series of samples, parameters for the presaturation sequence must often be re-adjusted for each sample. The EXCEPT (EXponentially Converging Eradication Pulse Train) presaturation pulse sequence was developed to eliminate time consuming pulse-parameter re-optimization as long as the variation in the solvent's $T_1$ remains within an order of magnitude. EXCEPT consists of frequency-selective inversion pulses with progressively decreasing interpulse delays. The interpulse delays were optimized to encompass $T_1$ relaxation times ranging from 1 to 10 seconds, but they can be easily adjusted by a single factor for other ranges that fall within an order of magnitude with respect to $T_1$. Sequences with different numbers of inversion pulses were tested to maximize suppression while minimizing the number of pulses and thus the total time needed for suppression. The EXCEPT-16 experiment, where 16 denotes the number of inversion pulses, was found satisfactory for many standard applications. Experimental results demonstrate that EXCEPT provides effective $T_1$-insensitive solvent suppression as predicted by the theory. The robustness of EXCEPT with respect to changes in solvent $T_1$ allows NMR investigations to be carried out for a series of samples without the need for pulse-parameter re-optimization for each sample.

# 1. INTRODUCTION

For our research in hydrothermal biomass-to-fuel (BTF) reactions of lignocellulosic biomass, quantitative proton NMR has proven to be a more expedient and accurate method for analysis of kinetics and mechanisms than the more commonly used HPLC technique. As with most large biomolecules, BTF compounds are often studied in aqueous solution. However, the overwhelming 110 M $^{1}$H solvent signal can impede these investigations particularly when quantitative information is desired (1-4). If the receiver gain is set low enough to avoid analog-to-digital converter (ADC) overflow by the solvent magnetization then the dynamic range available to resolve the solute signals is limited. Even if the solute signals can be adequately resolved, the magnitude of the solvent signal may still obscure solute signals close to the solvent resonance. A common solution to the limitations imposed by a protic solvent is the substitution with a deuterated solvent. However, this is impractical for substances that are naturally dissolved in water or react to produce water as a by-product, such as with biomolecules and BTF compounds. In addition, accelerated proton-deuteron exchange occurs during hydrothermal BTF conversions at elevated temperatures due to multiple keto-enol tautomerisms which also obstructs quantitative NMR analysis.

There is already a wide variety of solvent suppression techniques available(2). Nonetheless, the challenge here is not simply to suppress a large solvent signal, but to do so for a series of samples that vary in $T_1$. During hydrothermal BTF reactions the pH of the solution fluctuates significantly as a result of acidic and basic by-products. Additives such as inorganic salts and mineral acids that are used to optimize the desired product yields cause additional variations in the pH of the solution. These factors significantly

alter the longitudinal relaxation rates of the solvent protons over the course of the reaction, which can affect the ability of an NMR sequence to suppress the solvent signal. An ideal suppression sequence would require minimal re-optimization of pulse-sequence parameters between samples, exhibiting robustness with respect to large variations in the longitudinal relaxation rates for the solvent protons.

Some of the most common solvent suppression sequences – CW presaturation, WATERGATE (WATER suppression by GrAdient-Tailored Excitation), WET (Water suppression Enhanced through $T_1$ effects) and PURGE (Presaturation Utilizing Relaxation Gradients and Echoes) – were considered to find a sequence that fulfils the demands of hydrothermal BTF analysis. CW presaturation is one of the most straightforward methods of solvent suppression, however, this method is subject to baseline distortions and the soft-pulse frequency requires re-adjustment when the solvent signal's resonance frequency changes for different samples. WATERGATE is said to provide "pure phase" spectra without baseline distortions(5) and can be tailored to a narrow suppression region to reduce its effect on surrounding peaks(6). However, it is still too sensitive with respect to the $T_1$ fluctuations present in BTF investigations. WET is reportedly less $B_1$- and $T_1$-sensitive(7, 8), but its tolerance of $T_1$ variations is still too narrow for fast and convenient NMR investigations of BTF samples. PURGE is reported to result in highly selective suppression with flat baselines and excellent phase properties (9), however, solvent suppression pulse sequences that use CW soft pulses suffer from a loss of quantitative signal information if solute protons are in exchange with solvent protons. The EXCEPT (EXponentially Converging Eradication Pulse Train) sequence introduced here provides a viable alternative for solvent suppression, tolerating at least an

order of magnitude variation in solvent $T_1$'s while maintaining quantitative signal information. It uses only delays and selective inversion pulses without the need for multiple channels, gradients, or adjusting power levels.

## 2. THEORY OF EXCEPT

EXCEPT is a pulse train of selective inversion pulses, such as adiabatic hyperbolic secant pulses (sech pulses)(10), with progressively decreasing interpulse delays. It follows the concept of multiple inversion-recovery nulling (11, 12) and was inspired by earlier approaches utilizing aperiodic pulse trains for saturation of magnetization (13, 14). Figure 1 shows the timeline of EXCEPT-16, which is an EXCEPT sequence of 16 pulses and 16 interpulse delays. Also shown in Fig. 1 are two longitudinal magnetization recovery curves (depicted in red and blue) of equal initial magnitude as they evolve through the inversion and recovery periods in the sequence. Although the $T_1$ time constants differ by a factor of five the sample magnetizations are similarly suppressed at the conclusion of the sequence. The interpulse periods in Fig. 1 are adjusted to suppress magnetization within an order of magnitude in $T_1$. This renders EXCEPT extremely robust for signal suppression with a high tolerance for variations in $T_1$.

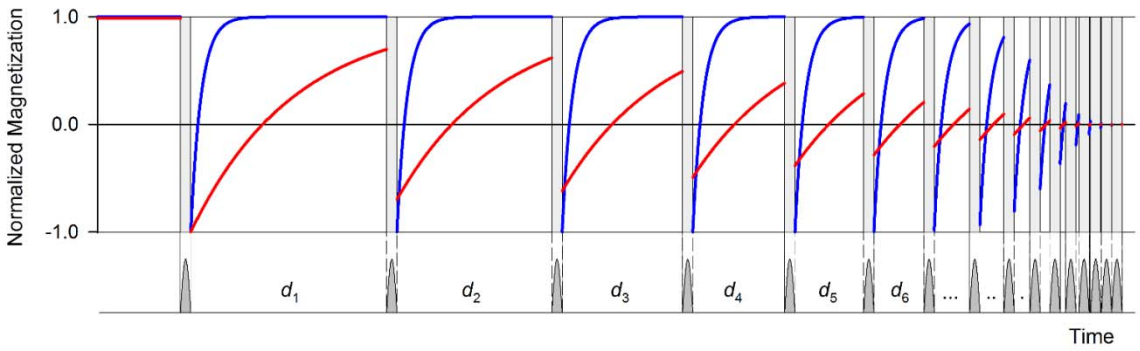


Figure 1. Timing of the EXCEPT-16 selective inversion pulses and interpulse delays (lower part) for effective suppression of longitudinal magnetization. Two sample magnetizations (upper part) with $T_1$ time constants that differ by a factor of five are equally suppressed to zero by the end of the pulse sequence.

The progressively decreasing delays $d_i$, where $i$ denotes the delay following the $i^{th}$ pulse (Fig. 1), were calculated according to the recursive formula

$$d_i = d_n\,(n-i+1)^x \qquad (1)$$

where $x$ is the exponent of convergence and $n$ is the number of inversion pulses in the sequence, i.e., $n$ = 16 for EXCEPT-16.

In an alternating least-squares procedure (15), $d_n$ and $x$ were iteratively optimized to cover $T_1$ times from 1 to 10 s (Table 1). The optimized exponents of convergence were found to be $x$ = 2.95, 3.65, 3.89, and 4.01 for EXCEPT-12, EXCEPT-16, EXCEPT-20, and EXCEPT-24, respectively, resulting in least-squares deviations from complete signal suppression of $\chi^2 = 1.4 \times 10^{-5}$, $2.4 \times 10^{-7}$, $3.5 \times 10^{-9}$, and $4.9 \times 10^{-11}$, respectively.

Because solvent suppression does not need to be executed on fully relaxed magnetization, EXCEPT can utilize the relaxation delay between consecutive scans by beginning to suppress solvent signals immediately after data acquisition. For example, if the solvent $T_1$ is suspected to be between 1 and 10 s then a relaxation delay of 50 s ($5 \times T_1$) would normally be implemented. EXCEPT-16 for this $T_1$ range requires 75 s to be fully executed, thus extending the relaxation delay by 50%.

To further illustrate how EXCEPT acts on magnetizations with different relaxation time constants, Fig. 2 shows a linear plot (Fig. 2a) and a semi-log plot (Fig. 2b) of the longitudinal magnetization that remains at the end of each interpulse delay $d_i$ of EXCEPT-16 as a function of $T_1$. A salient feature of Fig. 2a is the change in curvature of the magnetization traces as the sequence progresses. With each additional delay from $d_1$ to $d_7$, the point of inflection in the traces shifts to lower $T_1$ relaxation time constants. The

magnetization inverts from negative to completely positive curvature after $d_7$ which was found to be essential for the sequence to be successful.

Table 1. Interpulse delays optimized for the suppression of longitudinal magnetization with relaxation time constants, $T_1$, within the range of 1 – 10 s.

| Interpulse delays (s) | | | | |
|---|---|---|---|---|
| Delay | EXCEPT-12 | EXCEPT-16 | EXCEPT-20 | EXCEPT-24 |
| $d_i$ | x = 2.95 | x = 3.65 | x = 3.89 | x = 4.01 |
| $d_1$ | 17.12268 | 18.88342 | 20.47159 | 21.28725 |
| $d_2$ | 13.24374 | 14.92077 | 16.76581 | 17.94438 |
| $d_3$ | 9.995602 | 11.59956 | 13.58337 | 15.01201 |
| $d_4$ | 7.323546 | 8.850851 | 10.87336 | 12.45500 |
| $d_5$ | 5.172570 | 6.608794 | 8.587350 | 10.23979 |
| $d_6$ | 3.487383 | 4.810769 | 6.679394 | 8.334415 |
| $d_7$ | 2.212361 | 3.397455 | 5.106032 | 6.708471 |
| $d_8$ | 1.291496 | 2.312937 | 3.826320 | 5.333143 |
| $d_9$ | 0.668329 | 1.504821 | 2.801848 | 4.181196 |
| $d_{10}$ | 0.285851 | 0.92437 | 1.996757 | 3.226971 |
| $d_{11}$ | 0.086352 | 0.526655 | 1.377762 | 2.446384 |
| $d_{12}$ | 0.011157 | 0.270743 | 0.914176 | 1.816926 |
| $d_{13}$ | --- | 0.119919 | 0.577939 | 1.317663 |
| $d_{14}$ | --- | 0.041969 | 0.343642 | 0.929231 |
| $d_{15}$ | --- | 0.009556 | 0.188568 | 0.633835 |
| $d_{16}$ | --- | 0.000762 | 0.092725 | 0.415249 |
| $d_{17}$ | --- | --- | 0.038896 | 0.258813 |
| $d_{18}$ | --- | --- | 0.012691 | 0.151429 |
| $d_{19}$ | --- | --- | 0.002618 | 0.081562 |
| $d_{20}$ | --- | --- | 0.000176 | 0.039234 |
| $d_{21}$ | --- | --- | --- | 0.01602 |
| $d_{22}$ | --- | --- | --- | 0.005049 |
| $d_{23}$ | --- | --- | --- | 0.000992 |
| $d_{24}$ | --- | --- | --- | 0.000061 |

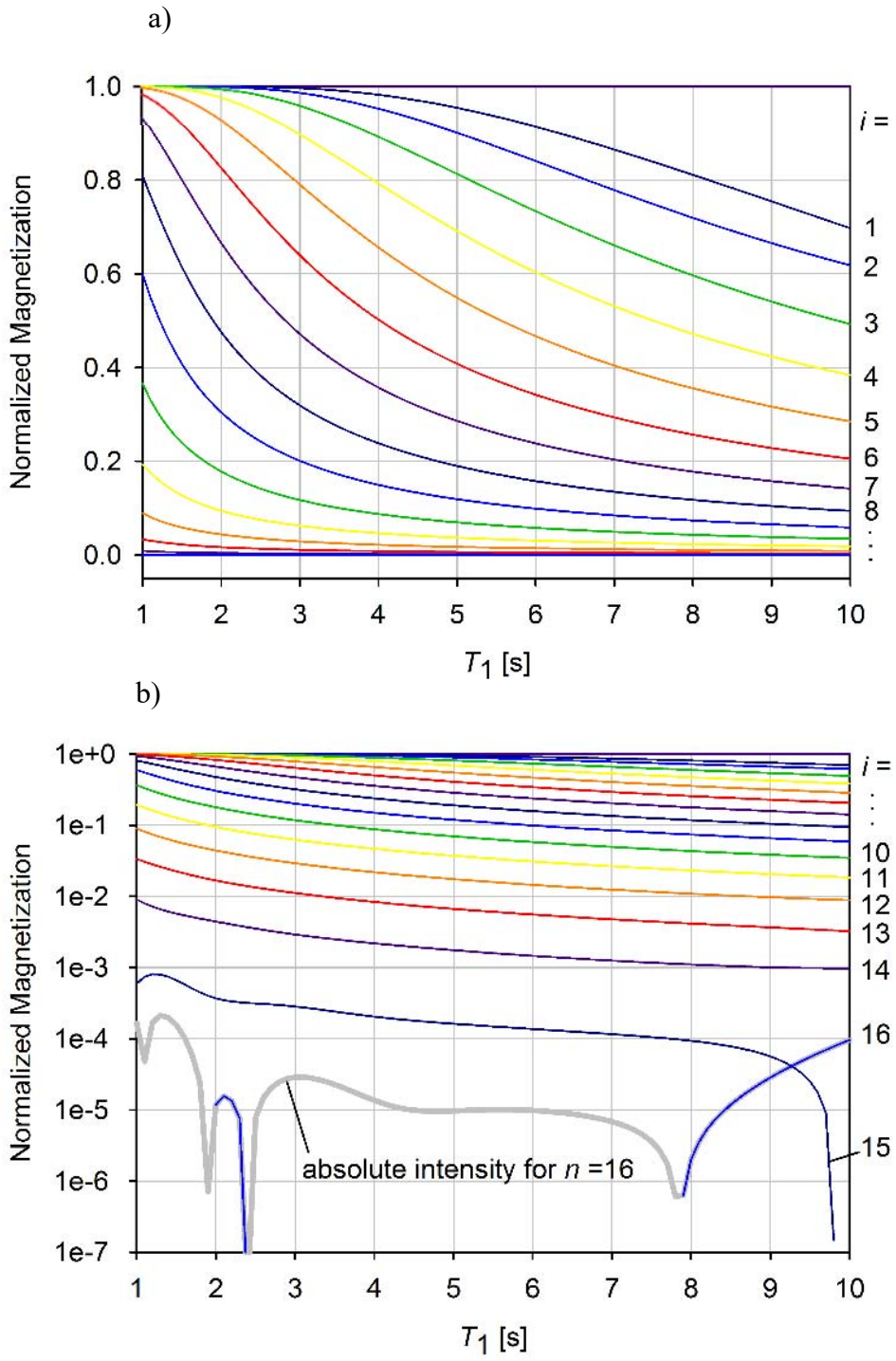


Figure 2. Residual longitudinal magnetization after each interpulse delay $d_i$ of EXCEPT-16 as a function of $T_1$. The $T_1$ axis covers the range for which suppression of magnetization was optimized: a) linear plot showing the effects of the early delays, b) semi-log plot showing effects of the final delays.

While EXCEPT was originally optimized to suppress solvent signals with relaxation time constants within the range 1 – 10 s, it may easily be adjusted to cover different ranges of $T_1$. A factor for delay adjustment (delay adjustment factor, $f_{da}$) is used to adjust each interpulse delay $d_i$ such that Eq. (1) changes to

$$d_i = f_{da} [d_n (n\text{-}i\text{+}1)^x] \quad (2)$$

This adjustment changes the $T_1$ range of optimal signal suppression from 1 – 10 s to the range $f_{da}\times 1$ s to $f_{da}\times 10$ s. For instance, if the solvent's $T_1$ value is expected to be within the range 0.5 – 5 s, it is recommended to set $f_{da} = 0.5$ cutting all interpulse delays listed in Table 1 in half. Figure 3 provides a useful tool for estimating the value of the delay adjustment factor, where the grey-shaded area corresponds to the optimized range of solvent signal suppression. For example, $f_{da} = 0.28$ can be used to suppress solvent signals in routine $^1$H-NMR investigations of small molecules in aqueous solutions where the solvent's longitudinal relaxation times are typically within the range 0.28 – 2.8 s. Other ranges include $f_{da} = 1$ for samples of small molecules dissolved in degassed organic solvents, $f_{da} = 0.2$ for most biological samples from adipose tissue ($T_1 \approx 240$ ms) to blood ($T_1 \approx 1350$ ms), and $f_{da} = 0.015$ for larger biomolecules or small soluble polymers in acidic solutions where $T_1$ is typically within 15 - 150 ms.

The calculations indicate that an increased number of inversion pulses and interpulse delays in the EXCEPT sequence (i.e., changing the presaturation sequence successively from EXCEPT-12 to EXCEPT-16, EXCEPT-20, and EXCEPT-24) leads to better solvent suppression in the final spectrum. However, due to the very short durations of the later delays in EXCEPT-20 and EXCEPT-24 (i.e., interpulse delays that are shorter than 1 ms, while the selective inversion pulse might last longer than 100 ms), neglecting

relaxation during inversion pulses in the calculations might no longer produce accurate results. Furthermore, instrumental limitations may make it difficult to manifest the full efficacy of EXCEPT in an NMR experiment where short delays are combined with long selective inversion pulses.

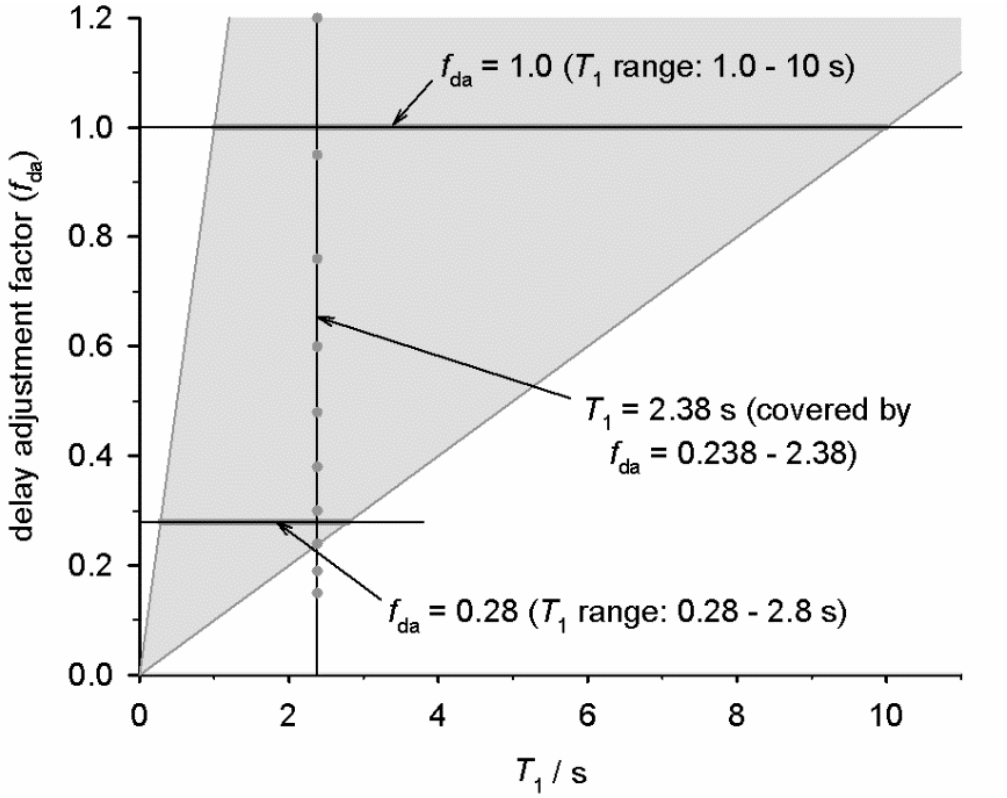


Figure 3. Ranges of $T_1$ for which EXCEPT successfully suppresses solvent signals (grey-shaded area) as a function of the delay adjustment factor ($f_{da}$). The $T_1$ range can easily be adjusted by changing the $f_{da}$. While $f_{da} = 1$ covers $T_1$ range = 1 – 10 s, $f_{da} = 0.28$ should be used if the solvent's $T_1$ falls within the range 0.28 – 2.8 s (horizontal lines). On the contrary, a solvent relaxation time of $T_1 = 2.38$ is sufficiently suppressed by any $f_{da}$ value that lies between 0.238 and 2.38 (vertical line).

# 3. RESULTS AND DISCUSSION

All NMR experiments were carried out at room temperature with a 400-MHz Varian Inova spectrometer employing a standard 5-mm broad-band probe. No post-acquisition treatment was applied to any of the data shown.

The suppression range of EXCEPT was tested using EXCEPT-16 with a delay adjustment factor $f_{da} = 0.22$, which is optimized for suppression of signals with $T_1 = 0.22$ s to $T_1 = 2.2$ s. Spectra of the residual HDO resonance in $CuSO_4/D_2O$ solutions were recorded from samples with $T_1$ ranging from 0.121 s to 3.17 s. As can be seen in Fig. 4 the EXCEPT sequence is very robust with respect to solvent relaxation time constants that differ by more than an order of magnitude; samples with $T_1$ from 0.235 s to 2.39 s were suppressed by amounts greater than 99% in signal magnitude. Even solvent magnetizations with relaxation time constants outside the optimized range were reduced by 93% or more by the sequence.

The $T_1$ suppression range of EXCEPT-16 was also tested by adjusting the $f_{da}$, thus shifting the relaxation time suppression range, while analyzing a single sample with a solvent relaxation time of 2.98 s. The $f_{da}$ value was increased from 0.19 to 3.01, placing the actual $T_1$ value of the HDO protons at different positions within the optimized range of EXCEPT-16. The smallest $f_{da}$ value used in this series was 0.15 optimizing EXCEPT-16 suppression for solvent protons with longitudinal relaxation times from 0.15 s to 1.5 s, which is well below the $T_1$ of the tested sample. Similarly, the longest $f_{da}$ tested was 3.01, which results in an optimal suppression range of 3.01 s to 30.1 s.

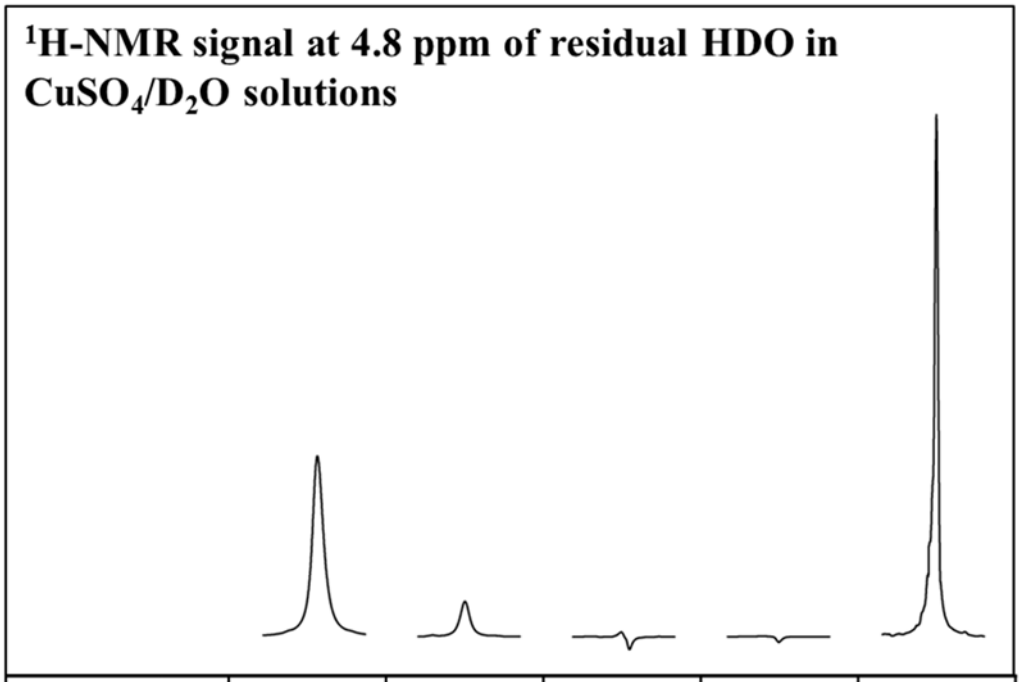


| $CuSO_4$/M | 0.0125 | 0.00625 | 0.00156 | 0 | 0 (deoxygenated) |
|---|---|---|---|---|---|
| $T_1$/s | 0.121 | 0.235 | 0.805 | 2.39 | 3.17 |
| % Suppression | 97.57 | 99.53 | 99.83 | 99.93 | 93.00 |

Figure 4. Residual HDO peaks versus $T_1$ following application of EXCEPT-16 solvent suppression pulse sequence.

Figure 5 shows a typical NMR spectrum of a sample containing maleic acid with an unsuppressed residual HDO solvent signal at 4.81 ppm. Fig. 6 displays the experimental results for the HDO solvent signal suppression for various $f_{da}$ values with the maleic acid proton signal unaffected. For $f_{da} = 0.30$ the residual water signal demonstrated greater than 97% reduction, and for $f_{da} = 2.39$ the residual water signal was suppressed greater than 99%. This shows effective solvent suppression by EXCEPT-16 for at least an order of magnitude variation in $T_1$, i.e., from $f_{da}$ to $10 \times f_{da}$.

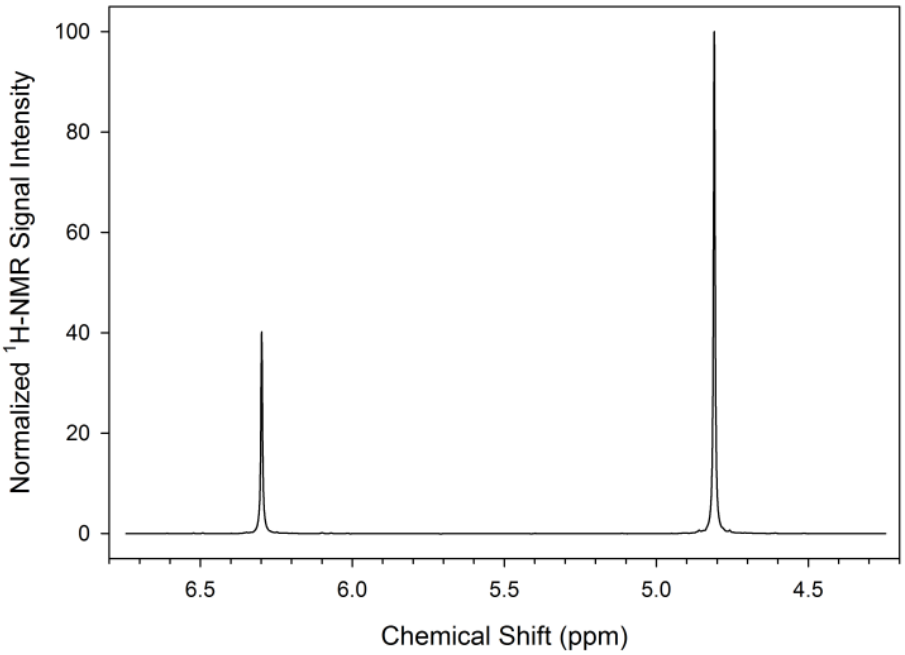


Figure 5. $^1$H NMR spectrum of 0.5 M maleic acid in 99.5% $D_2O$.

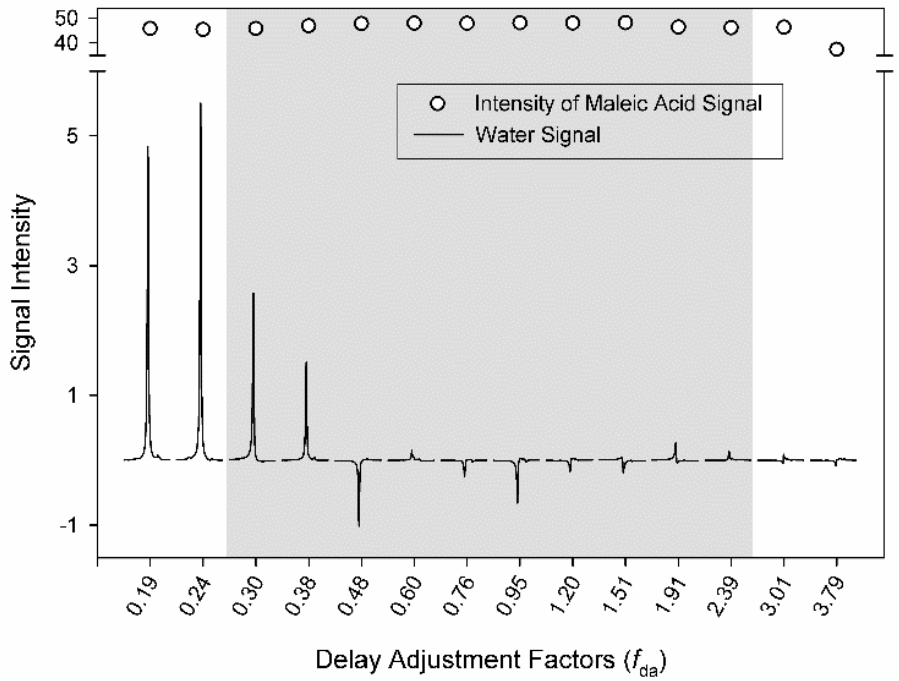


Figure 6. Residual water signal versus delay adjustment factor using EXCEPT-16 solvent suppression on 0.5 M maleic acid sample in 99.5% $D_2O$. The shaded area corresponds to $f_{da}$ values for which the $T_1$ falls within the optimized range.

A BTF sample with an HDO proton $T_1$ of 2.38 s was used in order to demonstrate EXCEPT-16 suppression on a sample for which the solvent suppression pulse sequence was originally devised. As shown in Fig. 7a, without solvent suppression the water signal impedes the analysis of the dilute BTF products; the analog-to-digital conversion cannot accurately represent the weak signals which are substantially distorted in the baseline as well as lost in the noise. Figure 7b shows the outstanding suppression along with the excellent baseline and phase properties that can be achieved with EXCEPT-16. For this sample, a sech pulse duration of 100 ms was chosen leading to the suppression bandwidth of 200 Hz. Comparison of the spectra in Fig. 7, specifically the peak at 5.05 ppm and the cluster of peaks at 4.50 ppm, reveals the potential of the EXCEPT-16 pulse sequence to reveal solute peaks near or under the wings of the solvent peak.

The EXCEPT-16 sequence resulted in an approximate 3000-fold reduction of the water signal intensity from Fig. 7a to Fig. 7b. Suppression factors were calculated using an external standard of 0.5 M maleic acid (1.0 M $^1$H)/99.9% $D_2O$ in a 1 mm capillary NMR tube as a basis for comparison between water signal magnitudes with and without the application of EXCEPT-16 suppression. These results were confirmed by directly comparing the absolute magnitude of the full water signal to that of the EXCEPT-16-suppressed signal. The receiver sensitivity was increased by a factor of 100 for the EXCEPT-16-suppressed spectrum (Fig. 7b), which was taken into account when comparing the magnitudes of the full and residual water signals.

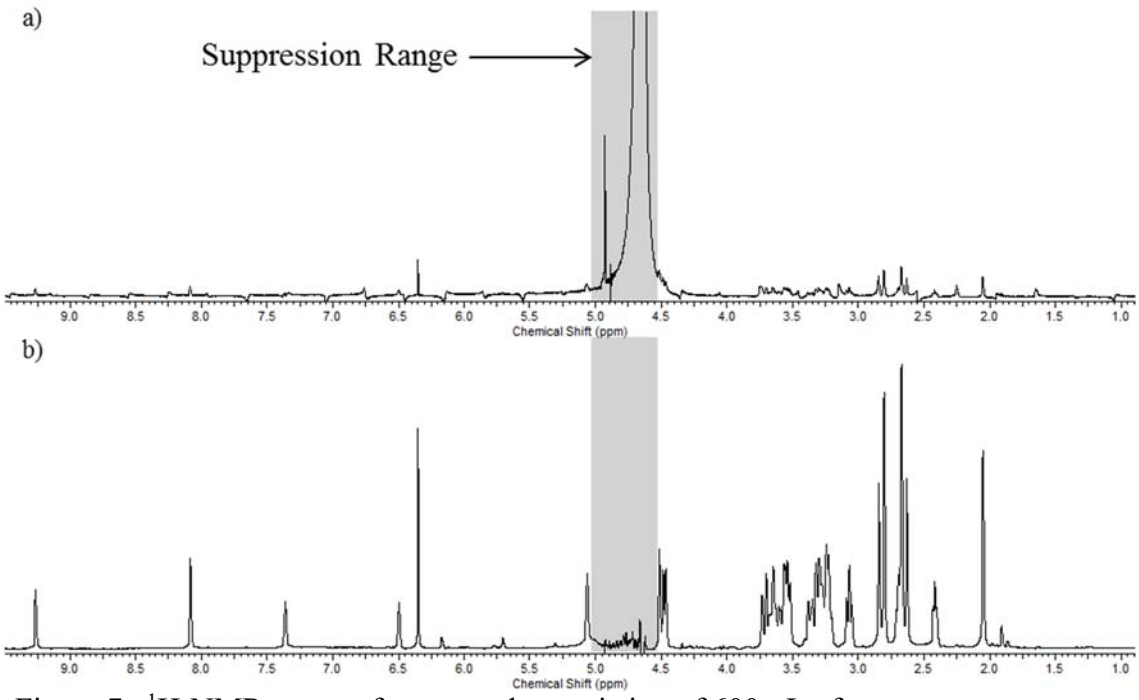


Figure 7. $^{1}$H-NMR spectra from sample consisting of 600 µL of room temperature solution taken from the reaction of 0.2 M D-glucose in citric acid buffer in a standard glass pressure vessel for 9 hours at 150°C. 150 µL of 99.5% $D_2O$ was added for a field-frequency lock. a) Spectrum obtained with 90° pulse (11 µs) and 16 scans. b) Spectrum obtained with EXCEPT-16 solvent suppression pulse sequence under an identical set of acquisition parameters.

# 4. CONCLUSION

The superior stability of EXCEPT suppression with respect to changes in solvent longitudinal relaxation time makes it possible to conduct $^{1}$H-NMR analysis on dilute samples with wide variation in $T_1$ without the need for re-adjustment of pulse sequence parameters between samples. Changing the $f_{da}$ parameter modifies the delay periods in the sequence, making it applicable for suppression of any desired range within an order of magnitude in $T_1$. Suggested values are $f_{da}$ = 0.28 for routine investigations of small molecules in aqueous solutions, $f_{da}$ = 1 for samples of small molecules dissolved in degassed organic solvents, $f_{da}$ = 0.2 for most biological samples from adipose tissue to blood, and $f_{da}$ = 0.015 for larger biomolecules or small soluble polymers in acidic solutions. EXCEPT may also be used as a general saturation sequence by replacing the frequency-selective soft pulses with hard pulses.

Original experiments with EXCEPT focused on a sequence with 20 pulses and 20 delays —EXCEPT-20; however, there was no improvement in suppression compared with EXCEPT-16. It was found that the maximum suppression predicted by the theory was not achieved, which was likely due to the long soft pulses versus the short delays at the end of the sequence. The pulse times were not accounted for in the optimization of the sequence even though they may allow for non-negligible relaxation of the solvent signal. The issue created by short delays coupled with long pulses becomes more pronounced as the delay adjustment factor becomes smaller which may result in less effective solvent signal suppression. Alternatively, a shorter duration for the soft pulse could be chosen leading to a wider than necessary suppression bandwidth.

Both simulated results and experimental observations demonstrate that EXCEPT's selective suppression is extremely tolerant of changes in the longitudinal relaxation time of solvent protons, with minimal adverse effects on the signals of interest. A suppression of 97% or more can be achieved over at least one order of magnitude of $T_1$ relaxation time constants regardless of where the actual value falls within the optimized $T_1$ range, while suppressing greater than 99% is accomplished over the majority of the $T_1$ suppression range. Greater than 94% suppression is still achieved when the actual $T_1$ value lies just above the optimized suppression range as well as greater than 99% suppression when the actual $T_1$ value falls somewhat below the optimized suppression range.

## REFERENCES


1. Hore PJ. Solvent Suppression. Methods in Enzymology. 1989:64-89.

2. Price WS. Water Signal Suppression in NMR Spectroscopy. Annual Reports on NMR Spectroscopy: Accademic Press Limited; 1999. p. 289-354.

3. Guéron M, Plateau P. Water Signal Suppression in NMR of Biomolecules. Encyclopedia of NMR: John Wiley & Sons, Ltd; 2012. p. 5383-94.

4. Krishnan VV, Murali N. Radiation Damping in Modern NMR Experiments: Progress and Challenges. Progres in Nuclear Magnetic Resonance Spectroscopy. 2013:41-57.

5. Hwang T-l, Shaka AJ. Water Suppression That Works. Excitation Sculpting Using Arbitrary Waveforms and Pulsed Field Gradients. Journal of Magnetic Resonance, Series A. 1995;112:275-9.

6. Liu M, Mao X-a, Ye C, Huang H, Nicholson JK, Lindon JC. Improved WATERGATE Pulse Sequences for Solvent Suppression in NMR Spectroscopy. Journal of Magnetic Resonance. 1998;132:125-9.

7. Smallcombe SH, Patt SL, Keifer PA. WET Solvent Suppression and Its Applications to LC NMR and High-Resolution NMR Spectroscopy. Journal of Magnetic Resonance, Series A. 1995;117:295-303.

8. Zhang S, Yang X, Gorenstein DG. Enhanced Suppression of Residual Water in a "270" WET Sequence. Journal of Magnetic Resonance. 2000;143:382-6.

9. Simpson AJ, Brown SA. Purge NMR: effective and easy solvent suppression. J Magn Reson. 2005;175(2):340-6.

10. Garwood TM. Adiabatic Pulses. NMR in Biomedicine. 1997;10:423-34.

11. Dixon WT, Sardashti M, Castillo M, Stomp GP. Multiple Inversion Recovery Reduces Static Tissue Signal in Angiograms. Magn Reson Med. 1991;18:257-68.

12. Mani S, Pauly J, Conolly S, Meyer C, Nishimura D. Background Suppression with Multiple Inversion Recovery Nulling: Applications to Projective Angiography. Magn Reson Med. 1997;37:898-905.

13. Dietrich W, Bergmann G, Gerhards R. Neues Verfahren zur Bestimmung der Longitudinalen Relaxationszeit in der Kernresonanzspektroskopie (New Method for Determining the Spin-Lattice Relaxation Time in Nuclear Resonance Spectroscopy). Z Anal Chem. 1976;279:177-81.

14. Trautner P, Woelk K. Fast Chemical-Shift T1 Imaging in Toroid Cavities for the Structural Analysis of Gels and Emulsions. Appl Magn Reson. 2002;22:291-305.

15. Bro R, De Jong S. A Fast Non-Negativity-Constrained Least Squares Algorithm. Journal of Chemometrics. 1997;11:393-401.

# II. PREDICTING THE EFFECT OF RELAXATION DURING FREQUENCY-SELECTIVE ADIABATIC PULSES

## ABSTRACT

Adiabatic half and full passages are invaluable for achieving uniform, $B_1$-insensitive excitation or inversion of macroscopic magnetization across a well-defined range of NMR frequencies. To accomplish narrow frequency ranges with adiabatic pulses (< 100 Hz), long pulse durations at low RF power levels are necessary, and relaxation during these pulses may no longer be negligible. A numerical, discrete recursive combination of the Bloch equations for longitudinal and transverse relaxation with the optimized equation for adiabatic angular motion of magnetization is used to calculate the trajectory of magnetization including its relaxation during adiabatic hyperbolic secant pulses. The agreement of computer-calculated data with experimental results demonstrates that, in non-viscous, small-molecule fluids, it is possible to model magnetization and relaxation by considering standard $T_1$ and $T_2$ relaxation in the traditional rotating frame. The proposed model is aimed at performance optimizations of applications in which these pulses are employed. It differs from previous reports which focused on short high-power adiabatic pulses and relaxation that is governed by dipole-dipole interactions, cross polarization, or chemical exchange.

# 1. INTRODUCTION

Models to predict the behavior of magnetization during NMR pulse sequences are indispensable for parameter optimizations in a variety of applications such as selective solvent suppression sequences (e.g., BISEP, SWAMP, SSAP, EXCEPT) or *in vivo* imaging with surface coils (1-4). Many solvent suppression sequences, for example, employ adiabatic pulses to selectively manipulate solvent spins while leaving analyte spins undisturbed. Adiabatic pulses such as the basic hyperbolic secant pulse (HS1) follow radiofrequency (RF) phase and amplitude modulation functions designed to confer uniform excitations (adiabatic half passages, AHP) or inversions (adiabatic full passages, AFP) that, above a given threshold, are independent of $B_1$ inhomogeneities.(5) During standard hard pulses with durations on the order of five to ten microseconds, standard $T_1$ and $T_2$ relaxation is in most cases negligible and can be ignored when optimizing parameters for high-resolution NMR investigations. For the same reason, $T_1$ and $T_2$ relaxation has been ignored in previous reports about relaxation during short, high-power adiabatic pulses.(6) However, for applications in which frequency selectivity with bandwidths smaller than 100 Hz is desirable, such as in the solvent suppression sequence EXCEPT,(4) adiabatic pulses can last up to hundreds of milliseconds.(7) In this article, we therefore address the effects of $T_1$ and $T_2$ relaxation to predict the behavior of magnetization during these slow and selective AHPs or AFPs.(2, 3, 8, 9)

Thorough theoretical and empirical treatments of relaxation phenomena in the presence of $B_1$ fields are provided in the literature for both spin-lock conditions with long, low-power standard pulses and manipulations of magnetization with adiabatic pulses.(6, 10-12) The latter works are primarily concerned with short adiabatic pulses (<

10 ms) requiring a relatively high RF power to maintain the adiabatic condition ($\omega_{1,max}/2\pi$ ≈ several kHz). Relaxation during these pulses is governed primarily by dipolar interaction, cross polarization and chemical exchange. Theoretical treatments of relaxation during these short, high-power adiabatic pulses have led to time-dependent relaxation functions applied collinear and perpendicular to the rotating effective $B_1$ field ($B_{eff}$) utilizing a tilted doubly-rotating frame. However, during long, low-power adiabatic pulses applied to non-viscous, small-molecule solutions, standard $T_1$ and $T_2$ relaxation becomes the primary effect while dipole-dipole relaxation may be insignificant. Ignoring standard $T_1$ and $T_2$ relaxation during frequency-selective (FS) pulses lasting hundreds of milliseconds can lead to inaccurate results and may negatively impact the optimization of performance parameters for sequences in which these pulses are utilized.(1, 8) To facilitate performance optimizations of sequences employing FS adiabatic pulses, we developed a model that accounts for relaxation during these pulses in a different way. The method predicts angular motion and relaxation of magnetization after a FS adiabatic pulse using a semi-empirical knowledge of the time-dependent angular motion of $B_{eff}$ during the adiabatic passage, the $T_1$ and $T_2$ values for the species of interest and the adiabatic pulse duration. The model makes it possible to quickly and effectively predict relaxation of magnetization during FS adiabatic passages for non-exchanging spins in non-viscous, small-molecule solutions.

# 2. THEORY

## 2.1. ADIABATIC PULSES AND $B_1$ INSENSITIVITY

For an adiabatic pulse such as the basic hyperbolic secant pulse HS1, (5) $B_{\text{eff}}$ changes orientation throughout the duration of the pulse at an angular velocity $\mathrm{d}\alpha/\mathrm{d}t$, where $\alpha(t)$ is the angle between the longitudinal axis of the rotating frame ($z$ axis) and the $B_{\text{eff}}$ axis:

$$\alpha(t) = \tan^{-1}\left(\frac{\omega_1(t)}{\Delta\omega_0(t)}\right) = \tan^{-1}\left(\frac{B_1(t)}{\Delta B_0(t)}\right) \quad (1)$$

When $\alpha(t)$ changes continuously from 0° to 90°, an adiabatic excitation (AHP) is achieved, while a continuous change of $\alpha(t)$ from 0° to 180° leads to an adiabatic inversion (AFP). As long as the frequency $\omega_{\text{eff}}$ associated with $B_{\text{eff}}$ is much greater than the frequency of the angular motion of $B_{\text{eff}}$, the adiabatic condition is fulfilled.(7, 13)

$$|\omega_{\text{eff}}(t)| \gg |\mathrm{d}\alpha/\mathrm{d}t| \quad (2)$$

Under adiabatic conditions, the net magnetization $M$ will follow $B_{\text{eff}}$, and a uniform excitation or inversion is achieved across the frequency bandwidth of the adiabatic pulse.(3, 13) To test the validity of the adiabatic condition for the pulse used in the following investigations, a series of experiments was conducted with a 200 MHz Bruker AVANCE DRX spectrometer, measuring the longitudinal magnetization $M_z$ with a 90° observe pulse following the application of a 500 ms, 60 Hz bandwidth AFP HS1 pulse with varying RF power. Figure 1 shows that inversion of magnetization is reasonably effective across at least one order of magnitude in RF pulse power. In this figure, RF power is expressed in terms of a dampening factor in decibels (dB) applied to the maximum pulse power available for the spectrometer. For comparison, a rectangular hard pulse (90° pulse) at 3 dB dampening required a pulse width of 11.54 μs.

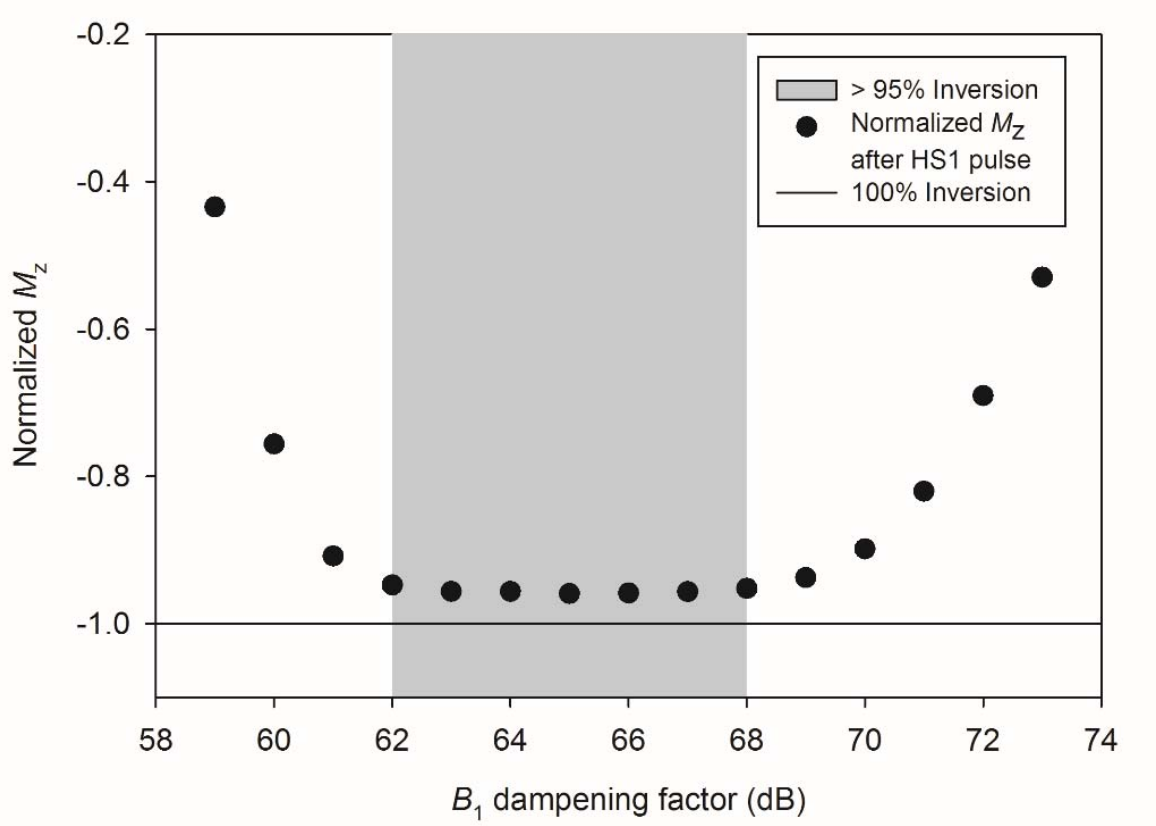


Figure 1. $B_1$ insensitivity of an adiabatic HS1 inversion pulse. The 1H NMR signal at 4.7 ppm from a 10% $H_2O$ sample in $D_2O$ (with a small amount of $CuSO_4$ added to achieve T1 = 1.95 s) was used to determine longitudinal magnetization after a 500 ms HS1 AFP with various power-level dampening factors. The experiments were performed on a 200 MHz Bruker AVANCE DRX spectrometer with a standard 5-mm broad-band probe. Incomplete inversion in the optimum range of 62-68 dB is attributed to relaxation during the HS1 pulse.

A model that utilizes the standard relaxation time constants $T_1$ and $T_2$ to predict the behavior of magnetization during adiabatic pulses must combine three time-dependent parametric equations: the Bloch equations for longitudinal and transverse magnetization (14) and the equation for the angular motion of magnetization (Eq. (1)). It is therefore important not only to know $T_1$ and $T_2$ but also the position of magnetization at any time during the pulse. However, $d\alpha/dt$ is only constant for very specific sets of time-dependent pulse amplitude and phase modulations. In the work described here, the

modulation functions result in slower angular motion at the beginning ($\omega_{eff} \approx \Delta\omega_{0,\,max}$) and end ($\omega_{eff} \approx -\Delta\omega_{0,\,max}$) of the pulse as compared to the middle of the pulse ($\omega_{eff} \approx \omega_{1,\,max}$). Achieving a constant $d\alpha/dt$ is rather difficult in an actual NMR investigation and will generally require extensive fine-tuning of the RF power level. On the contrary, it is quite unnecessary to go through the laborious process of fine-tuning because the adiabatic condition is fulfilled over a wide range of RF power levels (see Figure 1). For the remainder of the work described here, a dampening factor of 65 dB was used for the HS1 pulse, resulting in $\omega_{1,max}/2\pi$ around 20 Hz. The actual angular motion of magnetization was monitored in a series of experiments, and the angle $\alpha(t)$ determined from independent measurements of longitudinal and transverse magnetizations at different time points throughout the HS1 pulse (see "Experimental determination of M during AFP" described below). The experimental results for $\alpha(t)$ were compared to predicted values obtained from a least-squares optimization of Eq.(1), refining the relative amplitudes of $\omega_{1,\,max}$ and $\Delta\omega_{0,\,max}$ by a constant best-fit factor ($f_{bf}$). The optimized equation of angular motion, therefore, is given by Eq.(3) :

$$\alpha_{opt}(t) = \arctan\left[f_{bf} \times \frac{sin(\alpha_{th}(t))}{cos(\alpha_{th}(t))}\right] \qquad (3)$$

where $\alpha_{opt}(t)$ represents the angle of $B_{eff}$ at any time $t$ during the pulse and $\alpha_{th}(t)$ the angle assuming constant angular motion. The optimized angle $\alpha_{opt}(t)$ is then used for the discrete recursive computer calculation of magnetization during the adiabatic pulse (see Supplementary Materials).Figure 2 shows experimentally derived values for $\alpha(t)$ and the best fit from the least-squares optimization, indicating that the sample magnetization closely follows a predictable path of $B_{eff}$ as it traverses through 180° from $+z$ to $-z$. For

the best fit plotted in Figure 2, a best-fit factor of $f_{bf}$ = 0.3106 was determined for the RF power-level dampening of 65 dB (cf. Figure 1).

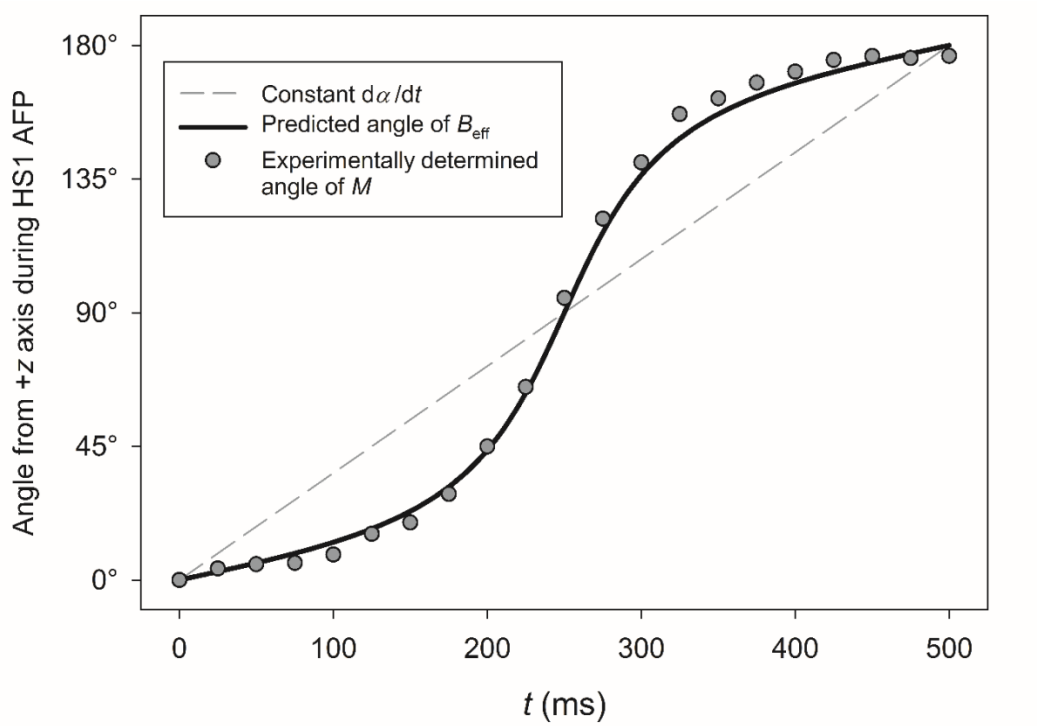


Figure 2. Orientation of $B_{eff}$ during a 500 ms HS1 AFP as a function of pulse duration. The filled circles indicate the orientation of magnetization derived from independent measurements of transverse and longitudinal magnetization components. The solid line shows the orientation calculated by a least-squares best-fit optimization of Eq. (1) to the experimental data ($f_{bf} = \omega_{1,\,max}/\Delta\omega_{0,\,max}$ = 0.3106). For reference, the dashed line represents constant angular motion.

With reliable data obtained for the angular motion of magnetization during the HS1 AFP, the mathematical approach presented here is able to predict relaxation during adiabatic pulses solely based on a first-order discrete recursive solution of the Bloch equations for longitudinal and transverse magnetization. It is noted that this method appears to be at odds with approaches in which relaxation during adiabatic pulses is

viewed as governed by time constants such as $T_{1\rho}$ and $T_{2\rho}$, i.e., by time constants for magnetization components oriented collinear and perpendicular to $B_{eff}$, respectively.(11, 12) In these approaches, magnetization relaxes continuously toward the origin of the moving $B_{eff}$ axis, and the relaxation rates $R_{1\rho}$ and $R_{2\rho}$ depend on the $B_{eff}$ field strength and direction.(15, 16) The method introduced here, however, is designed for long, low-power FS adiabatic pulses and does not propose to address the effects during short, high-power RF pulses where relaxation may be governed by dipole-dipole interactions, cross polarization or chemical exchange.(12) Hence, the method presented here is complementary to the aforementioned approaches and intended for close approximation of relaxation during FS adiabatic pulses in non-viscous, small-molecule solutions.

# 3. RESULTS AND DISCUSSION

## 3.1. SIMULATION OF MAGNETIZATION DURING AHP AND AFP

Because $T_1 \approx T_2$ in the extreme narrowing range of high-frequency $B_0$ fields, small-molecule samples, and low-viscosity solutions, $T_1$ and $T_2$ were assigned the same values in our computer simulations. The values for $T_1$ and $T_2$ can easily be adjusted individually in simulations for systems where these assumptions may no longer be valid. However, in ranges beyond the extreme narrowing limit (i.e., where $T_1$ and $T_2$ differ significantly from each other), other mechanisms such as dipole-dipole relaxation may need to be considered, and the model presented here must be expanded by the theory described in prior publications.(6, 11, 12, 15)

The calculation of angular motion and relaxation was conducted with a unit magnetization vector that initially is aligned parallel with the external magnetic field. The vector is then rotated from its original position at $t = 0$, where $M_z(t) = 1$ and $M_{xy}(t) = 0$, to the angular position of $B_{eff}(t)$ after a short, incremental time progress, $t + \Delta t$, utilizing the angle $\alpha(t + \Delta t)$ calculated from the HS1 amplitude and phase modulation functions and the refined relative amplitudes of $\omega_{1,\,max}$ and $\Delta\omega_{0,\,max}$ (Figure 2). After the incremental angular motion of the magnetization, standard longitudinal and transverse relaxation effects are calculated for $M_z$ and $M_{xy}$, respectively, using $T_1$, $T_2$, and the same short time increment $\Delta t$ as parameters. From the new components, $M_z(t + \Delta t)$ and $M_{xy}(t + \Delta t)$, the net magnitude of magnetization at $t + \Delta t$ is determined and placed in the direction of the next incrementally progressed angular position of $B_{eff}$. At the new angular position, the same incremental relaxation calculations is conducted for $M_z$ and $M_{xy}$. This stepwise recursive procedure is continued until $B_{eff}$ reaches its final position at the $-z$ axis of the

rotating frame. Accordingly, the duration of $\Delta t$ is given by the overall pulse width ($pw$) and the desired number of steps ($n$) in the calculation: $\Delta t = pw/n$. The value for $n$ determines the granularity of the resulting data, which should be sufficient to predict $M_z$ and $M_{xy}$ at or very close to time points of interest during the pulse. For the experiments described here, $n$ = 360 was used to provide simulation outputs corresponding to the nearest 1° of experimentally measured adiabatic angular motion. Larger values of $n$ were tested as well leading to an improvement in final amplitude prediction of 0.63% when using n = 3,600, and a further improvement of 0.04% with $n$ = 36,000. Figure 3 shows calculated trajectories of magnetization during a 500 ms HS1 AFP with various relaxation times ($T_1 = T_2$ = 0.65 s, 1.95 s, and 4.32 s). Furthermore, the trajectories in Figure 3 were extended as if the initial HS1 AFP would be following by a second 500 ms HS1 AFP in rapid succession. During the second AFP, the phase modulation function was modified such that $B_{eff}$ continues its rotation to ultimately complete a full 360° adiabatic passage. The inversion of magnetization calculated after the 180° AFP for samples relaxing at different rates is indicated by the circles on the $z$ axis in Figure 3. By comparison with the trajectory of no relaxation during the adiabatic passage (grey dashed line), it is evident that relaxation during a 500 ms HS1 AFP is substantial.

### 3.2. EXPERIMENTAL DETERMINATION OF *M* DURING AFP

To test the ability of the proposed model for predicting the behavior of net magnetization during adiabatic pulses, $M_{xy}$ and $M_z$ were measured at successive time points during the 500 ms HS1 AFP. The original HS1 AFP protocol supplied with the spectrometer's software was truncated at 20 evenly spaced time points throughout its duration, and $M_z$ and $M_{xy}$ components were determined in separate experiments for each.

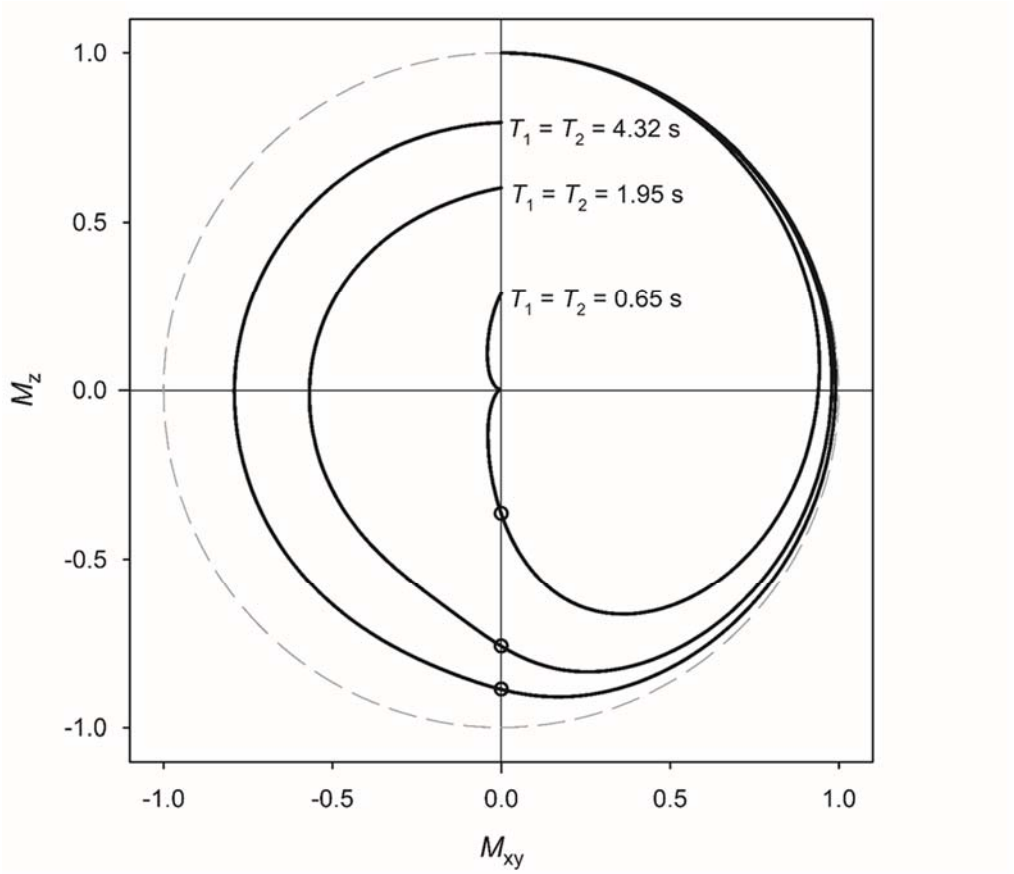


Figure 3. Trajectories of magnetization calculated from the angular motion of $B_{eff}$ during a 1,000 ms 360° adiabatic passage achieved by two successive 500 ms AFP HS1 pulses ($\omega_{1,\,max}/\Delta\omega_{0,\,max} = 0.3106$) while considering different set of $T_1$ and $T_2$ relaxation times ($T_1 = T_2 = 0.65$ s, 1.95 s, and 4.32 s). For reference, a trajectory of magnetization undergoing no relaxation is shown as a dashed line. The points of intersection with the $-z$ axis after the first 180° AFP are marked by open circles.

Longitudinal magnetization $M_z$ was measured by applying the truncated HS1 AFP pulses followed by a standard 90° observe pulse, effectively rotating the remaining $M_z$ into the $xy$ plane prior to acquisition. Transverse magnetization $M_{xy}$ was measured directly, i.e., without the application of an added observe pulse. A complete four-scan 90° phase cycle was used in both sets of experiments to accurately map the magnetization components. The experiments were performed using a 200 MHz Bruker AVANCE DRX spectrometer with a standard 5-mm broad-band probe. The sample solutions of different relaxation

times were composed of 90% $D_2O$, 10% $H_2O$, and varying small amounts of $CuSO_4$ as relaxation agent. The samples were placed in a 5-mm Shigemi tube (Shigemi Inc., Allison Park, PA, USA) at a maximum sample height of 10 mm, ensuring that the entire sample is confined to the region of homogeneous, maximum $B_1$ field. Calculated trajectories of net magnetizations with various relaxation times within the range expected for small molecules in non-viscous solutions (solid lines in Figure 4) are compared with magnetization values constructed from the $M_z$ and $M_{xy}$ components obtained experimentally by truncating the two consecutive 500 ms HS1 AFPs as described above. The representation in Figure 4 shows that the experimentally determined points on the path of $M$ during AFP nearly coincide with the simulated trajectories, especially for the first 180°. At the conclusion of the first 500 ms HS1 AFP, the magnitude of the calculated magnetization differs by about 10% from the magnitude determined by the experiments with samples relaxing at 0.65 s, 1.95 s, and 4.32 s. Consequently, the experimental relaxation rates appear to be slightly larger in each of the samples than predicted by $T_1$ and $T_2$ relaxation only. This may be due to additional relaxation effects driven by the applied $B_1$ field. Figure 4(a), where $T_1 = T_2 = 0.65$ s, provides clear evidence that longitudinal magnetization increases during the second 500 ms HS1 AFP after it had reached zero or close-to-zero magnetization. This effect is well explained by the relaxation model introduced here but may not be apparent from models that are solely based on relaxation toward the origin of the $B_{eff}$ axis.

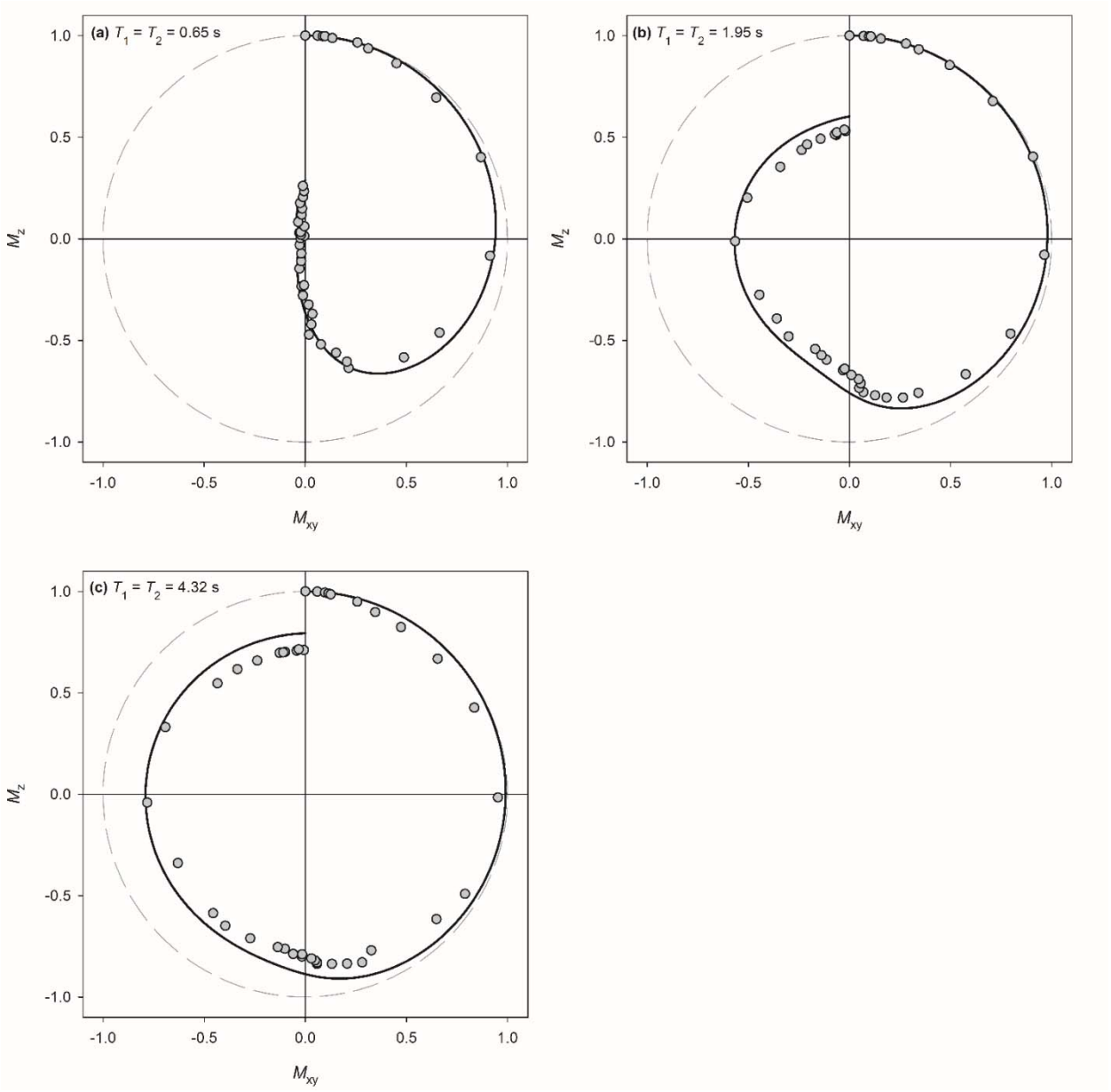


Figure 4. Comparison of calculated (solid line) and experimentally derived net magnetization (symbols) during two consecutive 500 ms, 60 Hz bandwidth HS1 AFPs for samples of 10% $H_2O$ in $D_2O$. Small amounts of $CuSO_4$ were added to the samples to adjust the relaxation times to the values indicated: **(a)** 0.65 s, **(b)** 1.95 s, **(c)** 4.32 s.

# 4. CONCLUSION

The development of the fast and approachable method presented here for predicting the behavior of net magnetization during FS adiabatic passages (AHP and AFP) indicates that relaxation during such pulses can be described reasonably well in terms of standard $T_1$ and $T_2$ relaxation. The new method is particularly useful for applications that depend on selective excitation or inversion of individual NMR resonances, such as solvent suppression sequences. (1-4). The prediction of net magnetization after a 90° or 180° adiabatic passage, or any other point during an adiabatic pulse, allows the user to better anticipate suppression performance, since these sequences are highly sensitive to variation in relaxation rate. (17, 18) Future directions will include modification of the calculation to potentially account for additional effects of the $B_1$ field strength on relaxation rates. The predictive power of the calculation should also be examined for large resonance offsets near the boundaries of the adiabatic bandwidth $\Delta\Omega$, coupled spin systems, and other commonly used adiabatic pulses such as $HS^n$ or CHIRP (19, 20). It is expected that upon determination of $\alpha(t)$ from best-fit analyses for these other modulation functions, the predictive model for relaxation during adiabatic angular motion can also be applied to these pulses.

# REFERENCES


1. De Graaf RA, Nicolay K. Adiabatic water suppression using frequency selective excitation. Magnet Reson Med. 1998;40(5):690-6.

2. De Graaf RA, Nicolay K. Adiabatic rf pulses: Applications to in vivo NMR. Concept Magnetic Res. 1997;9(4):247-68.

3. Garwood M, Uğurbil K. $B_1$ Insensitive Adiabatic RF Pulses. 1992:109-47.

4. Satterfield ET, Pfaff AR, Zhang W, Chi L, Gerald RE, 2nd, Woelk K. EXponentially Converging Eradication Pulse Train (EXCEPT) for solvent-signal suppression in investigations with variable T1 times. J Magn Reson. 2016;268:68-72.

5. Silver MS, Joseph RI, Hoult DI. Highly selective and π pulse generation. Journal of Magnetic Resonance (1969). 1984;59(2):347-51.

6. Sorce DJ, Michaeli S, Garwood M. Relaxation during adiabatic radiofrequency pulses. Current Analytical Chemistry. 2007;3(3):239-51.

7. Tannus A, Garwood M. Adiabatic pulses. NMR Biomed. 1997;10(8):423-34.

8. De Graaf RA, Luo Y, Garwood M, Nicolay K. B1-Insensitive, Single-Shot Localization and Water Suppression. Journal of Magnetic Resonance, Series B. 1996;113(1):35-45.

9. Degraaf RA, Luo Y, Terpstra M, Merkle H, Garwood M. A New Localization Method Using an Adiabatic Pulse, BIR-4. Journal of Magnetic Resonance, Series B. 1995;106(3):245-52.

10. Walbrecker JO, Hertrich M, Green AG. Accounting for relaxation processes during the pulse in surface NMR data. Geophysics. 2009;74(6):G27-G34.

11. Mangia S, Liimatainen T, Garwood M, Michaeli S. Rotating frame relaxation during adiabatic pulses vs. conventional spin lock: simulations and experimental results at 4 T. Magn Reson Imaging. 2009;27(8):1074-87.

12. Michaeli S, Sorce D, Garwood M. T2ρ and T1ρ Adiabatic Relaxations and Contrasts. Current Analytical Chemistry. 2008;4(1):8-25.

13. Garwood M, DelaBarre L. The return of the frequency sweep: designing adiabatic pulses for contemporary NMR. J Magn Reson. 2001;153(2):155-77.

14. Bloch F. Generalized Theory of Relaxation. Physical Review. 1957;105(4):1206-22.

15. Michaeli S, Sorce DJ, Idiyatullin D, Ugurbil K, Garwood M. Transverse relaxation in the rotating frame induced by chemical exchange. J Magn Reson. 2004;169(2):293-9.

16. Michaeli S, Sorce DJ, Springer CS, Jr., Ugurbil K, Garwood M. T1rho MRI contrast in the human brain: modulation of the longitudinal rotating frame relaxation shutter-speed during an adiabatic RF pulse. J Magn Reson. 2006;181(1):135-47.

17. Dixon WT, Sardashti M, Castillo M, Stomp GP. Multiple inversion recovery reduces static tissue signal in angiograms. Magnet Reson Med. 1991;18(2):257-68.

18. Mani S, Pauly J, Conolly S, Meyer C, Nishimura D. Background suppression with multiple inversion recovery nulling: Applications to projective angiography. Magnet Reson Med. 1997;37(6):898-905.

19. Bohlen JM, Bodenhausen G. Experimental Aspects of Chirp NMR Spectroscopy. Journal of Magnetic Resonance, Series A. 1993;102(3):293-301.

20. Tannús A, Garwood M. Improved Performance of Frequency-Swept Pulses Using Offset-Independent Adiabaticity. Journal of Magnetic Resonance, Series A. 1996;120(1):133-7.

## SUPPLEMENTARY MATERIAL

### MATLAB CODE FOR "PREDICTING THE EFFECTS OF RELAXATION DURING FREQUENCY-SELECTIVE ADIABATIC PULSES"

```
a=0:360;
%angle from positive z axis during pulse
sina=sind(a); cosa=cosd(a); a_th=0:9:360;
%angle of B_eff assuming constant angular motion
f_bf=sum(tan_th.*tan_exp)/sum((tan_th).^2);
%non-weighted LS optimization for orientation of B_eff
a_opt=atan2d(sina*f_bf,cosa);
for i=182:361
a_opt(i)=a_opt(i)+360;
end
%all a > 0 a_opt(361)=360; sinb=sind(a_opt);
cosb=cosd(a_opt);
%sin and cosine of optimized B_eff angles
t1=0.65; t2=0.65; pw=1.0;
%relaxation times and pulse width
[start,nsteps]=size(a);
%number of steps (n) dpw=pw/nsteps; relax1=exp(-dpw/t1);
relax2=exp(-dpw/t2);
%exponential decay for relaxation during (?t)
%to be applied to net magnetization mag=zeros(1,361);
trans_comp=zeros(1,361); trans_comp(1)=sinb(1);
%initial tranverse magnetization
longit_comp=zeros(1,361); longit_init=1;
longit_comp(1)=longit_init;
%initial longitudinal magnetization
for s=1:360
mag(s+1)=sqrt((trans_comp(s))^2+(longit_comp(s))^2);
trans_comp(s+1)=sind(a_opt(s+1))*mag(s+1);
longit_comp(s+1)=cosd(a_opt(s+1))*mag(s+1);
trans_comp(s+1)=(trans_comp(s+1))*relax2;
longit_comp(s+1)=1-(1-longit_comp(s+1))*relax1;
end
%for each step s, use net magnetization and optimized angle
from
%last step to determine longitudinal and transverse
components, then
%reduce components according to relaxation during dpw
(delta t).
```

# BLOCK DIAGRAM FOR SIMULATION PREDICTING THE EFFECT OF RELAXATION DURING FREQUENCY-SELECTIVE ADIABATIC PULSES

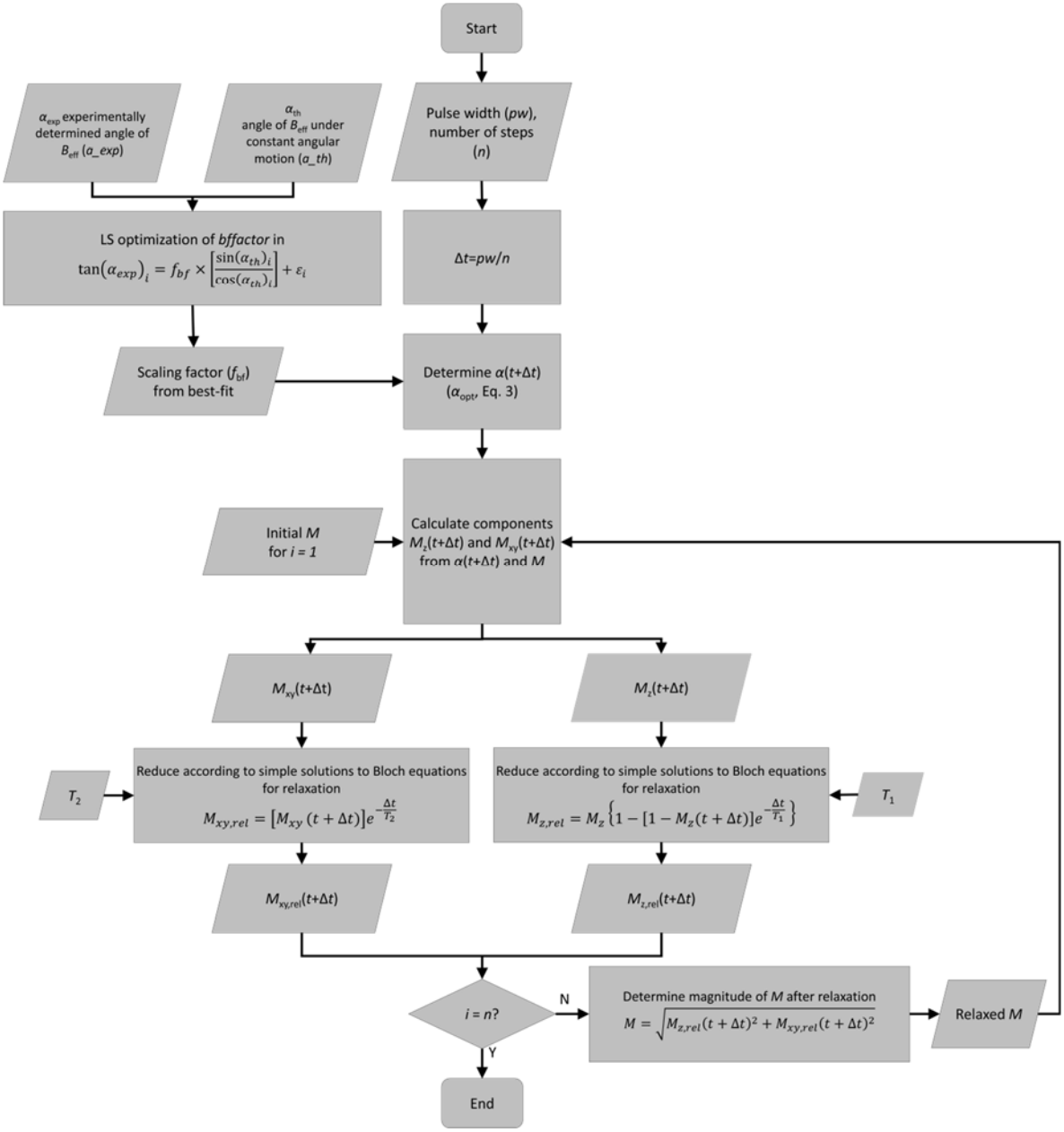

# III. A FAST AND CONVENIENT WAY TO PREDICT RELAXATION DURING A FREQUENCY-SELECTIVE ADIABATIC HYPERBOLIC SECANT PULSE (HS1 SECH PULSE)

## ABSTRACT

Frequency-selective inversion of magnetization is often achieved by long, low-power adiabatic RF pulses. Because these pulses can last hundreds of milliseconds, substantial relaxation of magnetization can occur during their application. Recently, a numerical model was introduced that allows an approximation of relaxation during frequency-selective adiabatic pulses for fast-tumbling small molecules in non-viscous solutions using only standard $T_1$ and $T_2$ relaxation times. This model is now extended to conditions in which net magnetization is not at its thermodynamic equilibrium prior to the adiabatic inversion. Simulated and experimental data reveal that the amplitude of net magnetization after an adiabatic inversion with the HS1 hyperbolic secant pulse can be approximated by a linear function of the magnetization before the pulse, depending only on $T_1$ and $T_2$ relaxation. The model presented here is particularly applicable to solvent-suppression sequences that utilize multiple adiabatic inversions, such as the multiple inversion-recovery nulling sequence EXCEPT. Tabulated slope and intercept values for the linear relationship are provided to facilitate a convenient optimization of pulse sequences that utilize HS1 frequency-selective adiabatic inversions.

# 1. INTRODUCTION

Relaxation during standard high-power RF pulses (hard pulses) is generally neglected in the theoretical treatments of NMR experiments because they are very short (5-20 μs) compared to the typical relaxation times of small molecules in non-viscous solutions. If adiabatic pulses are used instead, taking relaxation into consideration is no longer a trivial matter. Adiabatic pulses are phase- and amplitude-modulated RF pulses that confer stable inversion (or excitation, depending on the pulse) across a wide range of $B_1$ field strengths. Consequently, they are particularly attractive in applications where $B_1$ inhomogeneity is a primary concern, such as *in vivo* imaging.(1)

Relaxation during adiabatic fast passages has been addressed several times in the literature. (2-4) In the high-power $B_1$ fields of adiabatic fast passages, cross-relaxation due to dipolar interactions is the primary relaxation effect responsible for loss of signal intensity. However, these relaxation mechanisms are less relevant for low-power, frequency-selective (FS) adiabatic pulses, which utilize much smaller $B_1$ fields but last much longer. To address relaxation during FS adiabatic pulses for fast-tumbling analyte molecules in non-viscous solutions at high magnetic $B_0$ fields (i.e., small molecules for which the extreme narrowing limit applies), a basic numerical model was developed that reasonably well predicts evolution and relaxation of net magnetization during FS adiabatic passages based only on $T_1$ and $T_2$ relaxation. (5) This model is particularly useful to optimize parameters of sequences in which these pulses are used, and to predict to a large extent the loss or change of magnetization during these pulses. Particularly, in solvent-suppression sequences where low-power FS adiabatic pulses are applied to the resonance of water molecules, dipolar cross-relaxation mechanisms are not significant.

The work presented here is a further development that demonstrates the validity of the predictive model for magnetizations that are not fully relaxed, i.e., that are not at thermodynamic equilibrium of their nuclear spins. Specifically, a linear relationship was found between the net magnetization before and immediately after a low-power HS1 hyperbolic secant pulse.

# 2. THEORY

## 2.1. ADIABATIC PULSES

Adiabatic pulses differ from other shaped pulses in that their amplitude and phase (or equivalently, frequency) follow modulation functions that ensure a stable excitation or inversion across a designated spectral bandwidth $\Delta\omega_0$, provided the $B_1$ power exceeds a given threshold.(1)

$$\alpha(t) = \tan^{-1}\left(\frac{\omega_1(t)}{\Delta\omega_0(t)}\right) = \tan^{-1}\left(\frac{B_1(t)}{\Delta B_0(t)}\right) \quad (1)$$

The $B_1$ power threshold depends upon the rate of frequency sweep, i.e., faster sweeps will achieve wider $\Delta\omega_0$ ranges but require stronger $B_1$ fields to maintain the "adiabatic condition": (6)

$$|\omega_{\text{eff}}(t)| \gg |\mathrm{d}\alpha/\mathrm{d}t| \quad (2)$$

$$\gamma B_{\text{eff}}(t) = \omega_{\text{eff}}(t) = \sqrt{\omega_1(t)^2 + \Delta\omega_0(t)^2} \quad (3)$$

As long as the precession frequency $\omega_{\text{eff}}$ about the effective field $B_{\text{eff}}$ [Eq. (3)] is greater than the rate of angular motion ($\mathrm{d}\alpha/\mathrm{d}t$) from the $+z$ axis to the $-z$ axis for adiabatic inversions (or from the $+z$ axis to the $xy$ plane for adiabatic excitations) the net magnetization $M$ will "follow" the effective field of the pulse.(7) While the $B_1$ amplitude and phase modulations result in a reliable alignment of $M$ with the $-z$ axis in the standard rotating frame after inversion, the magnitude of the final magnetization ($M_{z,f}$) is often smaller than that of the initial equilibrium magnetization ($M_{eq}$) due to relaxation during the adiabatic pulse (5).

## 2.2. EXTENSION OF THE RELAXATION MODEL TO CONDITIONS IN WHICH $M_{Z,I} < M_{EQ}$

The need for robust solvent suppression with minimal adjustment between experiments motivated the use of FS adiabatic inversion pulses in the solvent suppression sequence EXCEPT.(8) The presaturation sequence EXCEPT is a train of FS inversion pulses with intervening delays based on the concept of multiple inversion-recovery nulling (9, 10). Magnetization within the selected frequency range undergoes multiple cycles of inversion and incomplete recovery until it approaches saturation and is effectively eliminated from the observed spectra. Computer-optimized recovery delays between the inversion pulses (interpulse delays) make it possible to suppress solvent magnetizations that vary in $T_1$ by more than an order of magnitude from sample to sample.(8) Because of its $B_1$ insensitivity and favorable inversion profile, the hyperbolic secant pulse HS1 (11) was chosen as the FS adiabatic inversion pulse for EXCEPT.

The interpulse delays of EXCEPT were computer-optimized based on data for the residual longitudinal magnetization before and after the FS inversion pulses.(8, 12) It is obvious that the consideration of relaxation throughout all elements of the EXCEPT sequence is crucial for successfully optimizing the delays. Nevertheless, only relaxation during the delays was accounted for in the early developments of EXCEPT, while relaxation during the rather long adiabatic inversion pulses (500 ms) was neglected. This quite common approach (13-15), however, led to calculated magnetizations that underwent less relaxation than their experimental counterparts, which relax during both delays and pulses. The discrepancy between experimental and theoretical treatment of relaxation during the HS1 pulse may have resulted in delays that were somewhat miscalibrated for the actual samples, although EXCEPT still produces superior

suppression regarding variations in $T_1$. (8) To further improve the performance of EXCEPT, it became necessary to consider relaxation during the FS pulses and develop a model that most accurately predicts the magnitude of $M$ after each inversion by including relaxation during the pulse. In the work described here, the model that was previously introduced for relaxation approximation during FS adiabatic HS1 pulses (5) is extended to cases where the net magnetization before the inversion ($M_{z,i}$) has not fully recovered to thermodynamic equilibrium of the nuclear spins ($M_{eq}$).

## 2.3. SIMULATION OF RELAXATION DURING FS ADIABATIC PULSES

Designed for investigations of small molecules in non-viscous solutions, where the extreme-narrowing limit applies, the model used here is detailed in (5). To predict the effects of relaxation and angular motion of $M$ during FS adiabatic pulses, the model uses three time-dependent parametric equations: the Bloch equations for longitudinal and transverse magnetization (16) and a modified equation for adiabatic angular motion. Because $\omega_1(t)$, and thus $\alpha(t)$ [Eq.(1)], at any given time $t$ during the adiabatic pulse depend on the $B_1$ field strength [Eqs. (2) and (3)], the equation of adiabatic angular motion is adjusted by a constant factor $f_{bf}$ obtained through a non-weighted least-squares analysis of experimentally measured pulse rotation angles of the net magnetization with respect to the $+z$ axis in the standard rotating frame:

$$\alpha_{opt}(t) = \tan^{-1}\left[f_{bf} \times \frac{sin(\alpha_{th}(t))}{cos(\alpha_{th}(t))}\right] \qquad (4)$$

Upon determination of $f_{bf}$, relaxation of $M$ is calculated as it follows $B_{eff}$ using a first-order discrete recursive solution to the Bloch equations for longitudinal and transverse magnetization. (5) For the model described in the previous work, this was accomplished by incrementally rotating a unit magnetization vector by an angle

$\alpha_{opt}(t+\Delta t)$ and subjecting its components $M_z$ and $M_{xy}$ to standard longitudinal and transverse relaxation for the same time interval ($\Delta t$), effectively modifying the amplitude of $M$. However, for the simulations described here, $M_z$ at $t = 0$ was set to approximately $0.25 \times M_{eq}$, $0.50 \times M_{eq}$, and $0.75 \times M_{eq}$ to correspond with experimentally determined magnitudes of $M$ following the partial recovery after a standard, non-adiabatic inversion. The resulting net magnetization was then progressed through the HS1 pulse by placing it at a new angle $\alpha_{opt}(t+\Delta t)$ and calculating the relaxation effects for the longitudinal and transverse magnetization components. The process was repeated until $\alpha_{opt}(t+\Delta t)$ reaches 180°, i.e., the end of the HS1 inversion pulse. For these simulations, $T_1$ was set equal to $T_2$ since the model was developed for samples in the extreme narrowing range.

# 3. RESULTS AND DISCUSSION

## 3.1. EXPERIMENTAL DETERMINATION OF *M* DURING INVERSION BY AN HS1 PULSE APPLIED AFTER INCOMPLETE RELAXATION ($M_{Z,I} < M_{EQ}$)

Experimental data were collected using a 5-mm broad-band probe in a Bruker Avance DRX-200 wide-bore spectrometer. Samples were composed of 10 % $H_2O$ in $D_2O$, and small amounts of relaxation agent ($CuSO_4$) were added to result in samples with various relaxation times typical for small molecules in non-viscous solutions (0.45 s, 0.86 s, and 2.28 s). The samples were used to evaluate the validity of the model when the water net magnetization before the adiabatic HS1 inversion was less than the equilibrium magnetization ($M_{z,i} < M_{eq}$). Longitudinal and transverse magnetizations during the adiabatic inversions were measured as described in (5). To achieve a longitudinal net magnetization smaller than $M_{eq}$ the magnetization at thermodynamic equilibrium was inverted from $+z$ to $-z$ by a 23-μs standard rectangular pulse and then allowed to recover partially before an adiabatic inversion pulse or portions thereof were applied. The recovery delays between the rectangular inversions and the adiabatic pulses were adjusted to yield about $0.25 \times M_{eq}$, $0.50 \times M_{eq}$, and $0.75 \times M_{eq}$.

For all experiments described herein, the HS1 pulse supplied with the spectrometer's software package (sech30.5, TopSpin 3.1, BRUKER Biospin) was used to investigate relaxation during adiabatic inversions. The full inversion pulse width was set to 250 ms to achieve a FS bandwidth of 120 Hz, with $\omega_{1,max}/2\pi$ at about 40 Hz to fulfill the adiabatic condition. At evenly spaced intervals throughout the pulse, longitudinal ($M_z$) and transverse ($M_{xy}$) magnetization components were measured separately to track the magnetization as it followed $B_{eff}$ from $+z$ to $-z$. To observe the position of *M* with

respect to the longitudinal axis and transverse plane during adiabatic inversion, the pulse was truncated at 20 equally spaced time points ($t_i$ = 0, 12.5, 25, … 250 ms); each successive point corresponds to rotation of $B_{eff}$ through a greater angle (i.e., $\alpha(t_i) < \alpha(t_{i+1}) \leq 180°$). To measure $M_z$, a standard 90° pulse was applied prior to acquisition, while the truncated HS1 pulse was followed directly by acquisition for the corresponding $M_{xy}$ determination. The investigations were repeated using three different samples of 10% $H_2O$ in $D_2O$ with $T_1$ relaxation times adjusted to 0.45 s, 0.86 s, and 2.28 s. Each experiment was conducted using a multiple of the 4-scan 90° phase-cycling routine to ensure faithful representation of the magnetization components in the resulting signal-averaged spectra. The data collected from each individual measurement were compared to the theoretical predictions described in section 2.3 (Figure 1).

### 3.2. ROBUSTNESS OF THE MODEL WITH RESPECT TO $B_1$ AND $M_{Z,I}$

In addition to varying the relaxation time, experiments were also conducted at different $B_1$-field power levels. Power levels were adjusted by the spectrometer software through attenuation values of 54 dB, 57 dB, and 60 dB. While the model offers a reasonable approximation for the path of magnetization during HS1 pulses (Fig. 1), the accuracy of simulation appears to be slightly impacted by the $B_1$ power level, with the best results achieved for samples subjected to attenuations of 57 dB or less. A change in $B_1$ power level leads to changes in the angular motion of magnetization from the $+z$ to the $-z$ axis as described in detail in ref. (6). At higher attenuation levels (i.e., lower $B_1$ power levels), the adiabatic angular motion of $B_{eff}$ is slower at the beginning and end of the HS1 pulse and faster at the center when the magnetization is close to the transverse plane. This effect is most pronounced at the $B_1$ dampening of 60 dB (C, F, and I in Fig. 1) where

experimentally measured magnetizations experience very little angular motion near the $+z$ and $-z$ axes, despite evident changes in the longitudinal component due to $T_1$ relaxation. The same behavior is seen in the simulated data (dashed lines), which shows that the best-fit factor $f_{bf}$ accurately scales longitudinal and transverse $B_{eff}$ components.

In the following, the relationship between $M_{z,i}$ and $M_{z,f}$ was explored in more detail. Simulations were performed using $M_{z,i}$ values between $0.01 \times M_{eq}$ and $M_{eq}$ for samples with relaxation times ($T_1 = T_2$) between 0.20 s and 5.00 s. Magnetizations $M_{z,f}$ are plotted as a function of $M_{z,i}$ for various relaxation times (Fig. 2), revealing strictly linear relationships above a minimum threshold value for $M_{z,i}$. Below this threshold, relaxation during the HS1 pulse yields $M_{z,f} = 0$ essentially eliminating all magnetization within the selected frequency range. Experimental evidence is shown in the inset, where $M_{z,i}$ for a sample with $T_1 = 0.45$ s was adjusted to less than $0.1 \times M_{eq}$ by inversion with a 180° hard pulse and partial recovery. The HS1 inversion that follows the partial recovery leads to complete elimination of magnetization in the simulation (solid line in the inset) and values close to zero for the experimentally measured magnetization (black filled circles). The most useful application envisioned for this special feature of adiabatic HS1 inversions is the effective destruction of unwanted magnetization.

A comparison between experimentally determined $M_{z,f}$ as a function of $M_{z,i}$ (filled symbols in Fig. 3) to simulated data (lines in Fig. 3) demonstrates that the model presented here provides a reasonable approximation of relaxation during adiabatic inversion, especially when the $B_1$ power level is sufficiently high and within the boundaries of the adiabatic condition. Experimentally determined magnetizations tend to relax slightly faster than predicted by the model, indicating that other relaxation

mechanisms may be present which are not addressed by the current model. Still, the model accounts for the majority of relaxation during low-power FS adiabatic HS1 inversions and, despite the discrepancy, the experimental and simulated data both exhibit the well-defined linear relationships between $M_{z,f}$ and $M_{z,i}$ depending only on the macroscopic $T_1$ and $T_2$ relaxation times:

$$M_{z,f} = aM_{z,i} + b \tag{5}$$

Because the linear relationship of Eq. (5) provides a convenient predictive tool for estimating the effects of relaxation during frequency-selective adiabatic HS1 pulses, the regression parameters $a$ and $b$ were calculated for relaxation times from 0.2 s to 5.0 s in increments of 0.05 s, with the best-fit factor $f_{bf}$ and the HS1 pulse width kept constant at 0.3 and 250 ms, respectively. The results of this calculation are plotted in Figure 4 and tabulated in Table 1. While the influence of $f_{bf}$ on $a$ and $b$ is negligible (see below), the pulse width scales directly with the relaxation time, i.e., values for $a$ and $b$ in Table 1 can be used for different pulse widths $pw' = c \times 250$ ms, if the same factor is applied to the relaxation time, i.e., $T_1' = cT_1$, where $T_1$ is the experimental relaxation time and $T_1'$ the value used for determining $a$ and $b$ in Table 1.

Calculation results as well as experimentally derived data show that the $B_1$ power level has a negligible effect on the relationship between $M_{z,i}$ and $M_{z,f}$. The three dashed lines in Fig. 5 depict trajectories calculated with the best-fit factors $f_{bf}$ for the $B_1$ dampening levels 54 dB, 57 dB, and 60 dB. The filled symbols represent experimental measurements of net magnetization at 0°, 90°, and 180° from the $+z$ axis for a sample relaxing at $T_1 = T_2 = 0.45$ s and inverted by a 250 ms HS1 pulse. The initial magnetization before the HS1 pulse ($0.5 \times M_{eq}$) was achieved by partial recovery after a

standard rectangular inversion pulse of 23 μs. While the trajectories are quite different for the three $B_1$ power levels, the final magnetization $M_{z,f}$ after completion of the HS1 inversion pulse is equal within the margins of experimental error (Fig. 5). The calculated values for $M_{z,f}$ also show only very minimal differences.

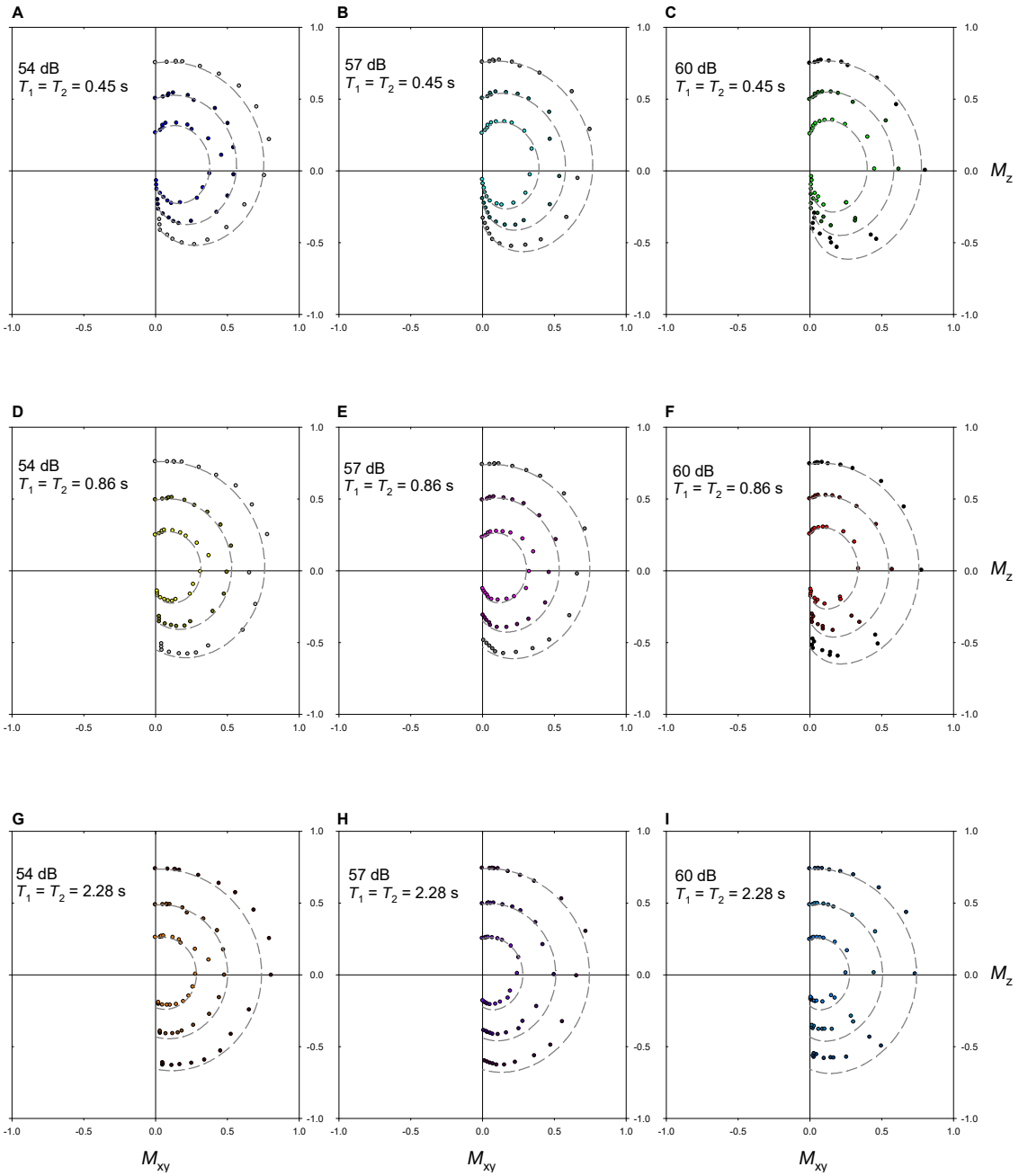


Figure 1. Simulated (dashed lines) and experimentally measured net magnetizations (filled circles) during adiabatic inversion for samples of 10% $H_2O$ in $D_2O$ with small amounts of $CuSO_4$ added to achieve relaxation times of 0.45 s (A-C), 0.86 s (D-F), 2.28 s (G-I). A 250 ms HS1 pulse with a 120 Hz bandwidth was used at $B_1$ power levels that correspond to the $B_1$ dampening factors: 54 dB (A, D, G), 57 dB (B, E, H), and 60 dB (C, F, I).

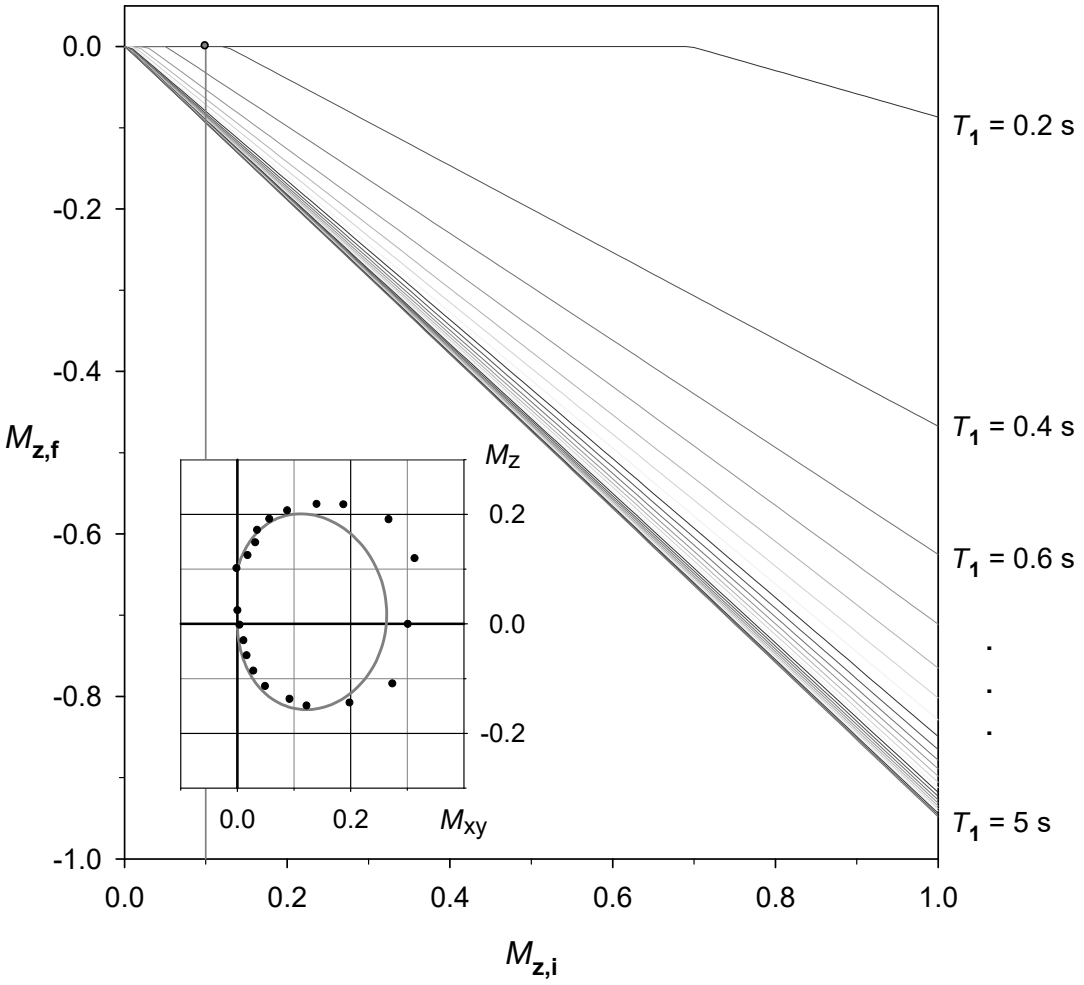


Figure 2. Final, normalized *z* magnetization ($M_{z,f}$) after an adiabatic HS1 inversion as a function of the normalized initial magnetization ($M_{z,i}$) before the HS1 pulse. A linear relationship between $M_{z,i}$ and $M_{z,f}$ is observed for magnetizations with relaxation times between 0.2 s and 5.0 s after a 250 ms adiabatic HS1 inversion. The inset shows an example of simulated (solid line) and experimental data (filled circles) for an initial magnetization ($M_{z,i} \approx 0.1 \times M_{eq}$, $T_1 = T_2 = 0.45$ s) that leads to saturation in $M_{z,f}$ (vertical line and filled circle in the main plot).

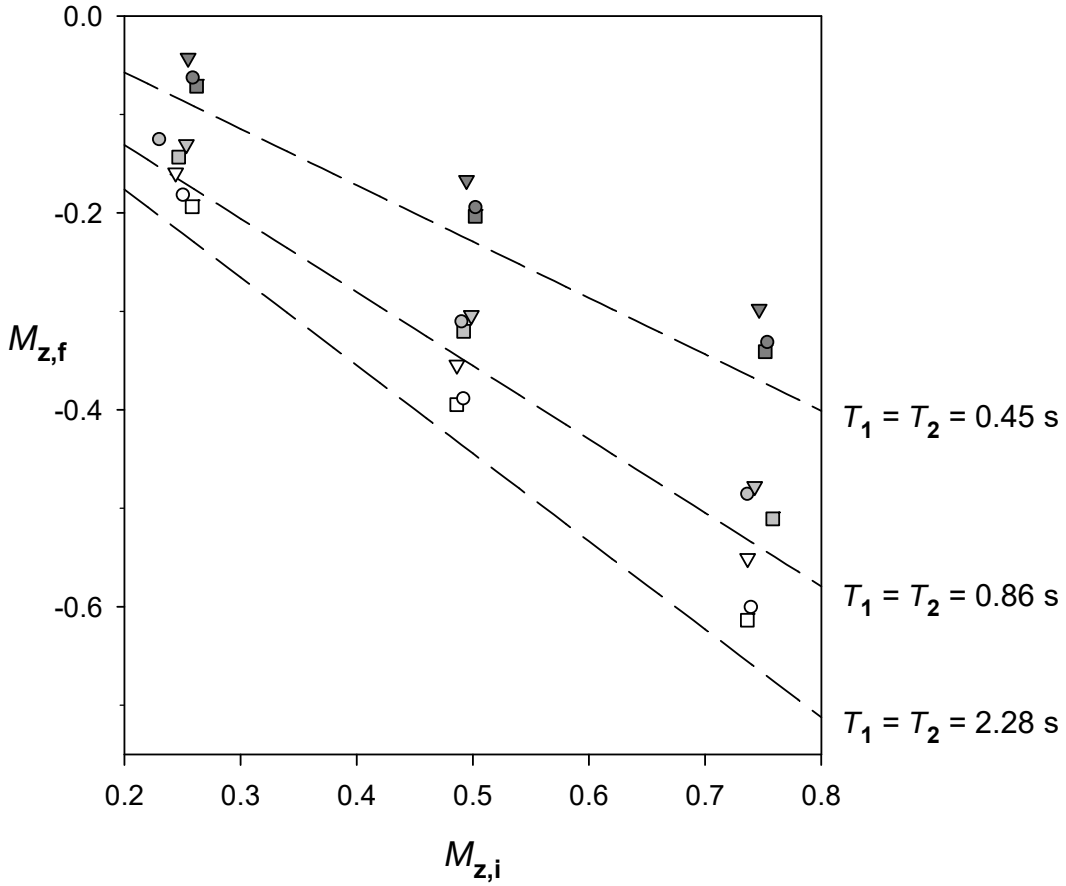


Figure 3. Comparison of predicted (dashed lines) and experimental (filled symbols) net magnetizations $M_{z,f}$ after a 250 ms adiabatic HS1 inversion of $M_{z,i}$. Experimental samples were composed of 10% $H_2O$ in $D_2O$ with small amounts of $CuSO_4$ added as relaxation agent.

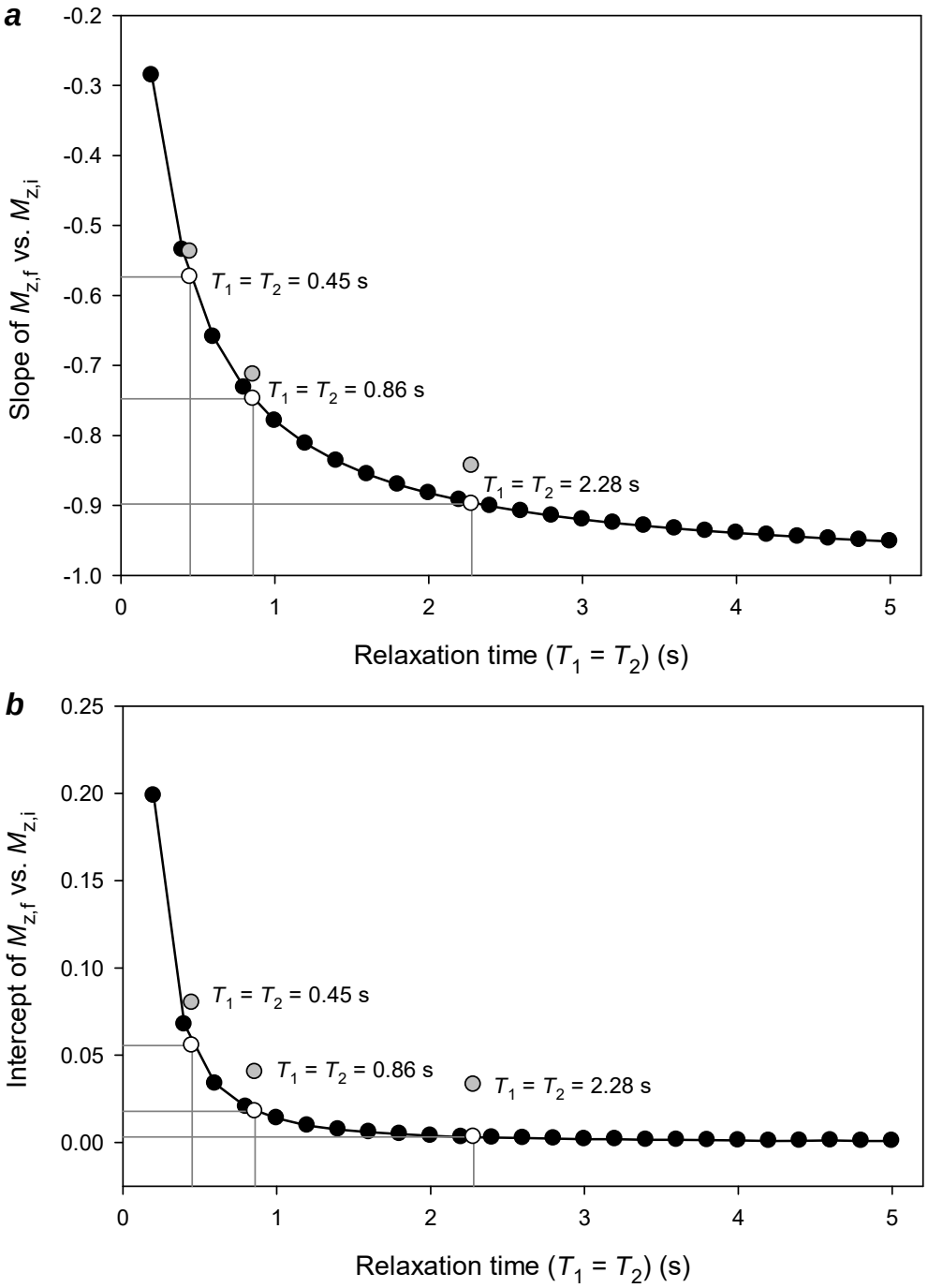


Figure 4. Regression parameters for linear range of $M_{z,f}$ vs. $M_{z,i}$ plots. Slope (A) and intercept (B) are shown (black filled circles) for plots of simulated net magnetizations before and after adiabatic inversion via 250 ms HS1 pulse, with relaxation times varying from 0.2 s to 5.0 s (as depicted in Figure 2). Parameters for linear regression analysis of simulated (white filled circles) and experimentally measured (gray filled circles) $M_{z,f}$ vs. $M_{z,i}$ with relaxation times of the experimental samples (0.45 s, 0.86 s, and 2.28 s) are shown as well.

Table 1. Linear regression parameters for $T_1$ (= $T_2$) from 0.20 s to 5.00 s

| $T_1 = T_2$ (s) | SLOPE | INTERCEPT |
|---|---|---|
| **0.20** | -0.2859 | 0.2086 |
| **0.25** | -0.3674 | 0.1502 |
| **0.30** | -0.4342 | 0.1131 |
| **0.35** | -0.4892 | 0.0882 |
| **0.40** | -0.5350 | 0.0708 |
| **0.45** | -0.5736 | 0.0581 |
| **0.50** | -0.6064 | 0.0486 |
| **0.55** | -0.6346 | 0.0412 |
| **0.60** | -0.6591 | 0.0354 |
| **0.65** | -0.6806 | 0.0307 |
| **0.70** | -0.6995 | 0.0269 |
| **0.75** | -0.7165 | 0.0239 |
| **0.80** | -0.7315 | 0.0213 |
| **0.85** | -0.7450 | 0.019 |
| **0.90** | -0.7574 | 0.0173 |
| **0.95** | -0.7685 | 0.0157 |
| **1.00** | -0.7788 | 0.0144 |
| **1.05** | -0.7881 | 0.0131 |
| **1.10** | -0.7967 | 0.0121 |
| **1.15** | -0.8046 | 0.0111 |
| **1.20** | -0.8119 | 0.0103 |
| **1.25** | -0.8186 | 9.54E-03 |
| **1.30** | -0.8250 | 8.94E-03 |
| **1.35** | -0.8310 | 8.42E-03 |
| **1.40** | -0.8365 | 7.85E-03 |
| **1.45** | -0.8417 | 7.42E-03 |
| **1.50** | -0.8465 | 6.94E-03 |
| **1.55** | -0.8511 | 6.55E-03 |
| **1.60** | -0.8554 | 6.22E-03 |
| **1.65** | -0.8595 | 5.89E-03 |
| **1.70** | -0.8632 | 5.48E-03 |
| **1.75** | -0.8669 | 5.25E-03 |
| **1.80** | -0.8702 | 4.89E-03 |
| **1.85** | -0.8736 | 4.76E-03 |
| **1.90** | -0.8767 | 4.51E-03 |
| **1.95** | -0.8798 | 4.43E-03 |
| **2.00** | -0.8825 | 4.15E-03 |
| **2.05** | -0.8853 | 4.02E-03 |
| **2.10** | -0.8877 | 3.77E-03 |
| **2.15** | -0.8905 | 3.88E-03 |
| **2.20** | -0.8927 | 3.55E-03 |
| **2.25** | -0.8947 | 3.27E-03 |
| **2.30** | -0.8970 | 3.21E-03 |
| **2.35** | -0.8991 | 3.12E-03 |
| **2.40** | -0.9011 | 3.01E-03 |
| **2.45** | -0.9030 | 2.89E-03 |
| **2.50** | -0.9049 | 2.88E-03 |
| **2.55** | -0.9067 | 2.74E-03 |
| **2.60** | -0.9083 | 2.58E-03 |
| **2.65** | -0.9100 | 2.50E-03 |
| **2.70** | -0.9116 | 2.45E-03 |
| **2.75** | -0.9131 | 2.32E-03 |
| **2.80** | -0.9146 | 2.29E-03 |
| **2.85** | -0.9160 | 2.19E-03 |
| **2.90** | -0.9174 | 2.16E-03 |
| **2.95** | -0.9188 | 2.11E-03 |
| **3.00** | -0.9200 | 2.00E-03 |
| **3.05** | -0.9213 | 1.96E-03 |
| **3.10** | -0.9225 | 1.90E-03 |
| **3.15** | -0.9237 | 1.85E-03 |
| **3.20** | -0.9248 | 1.73E-03 |
| **3.25** | -0.9260 | 1.79E-03 |
| **3.30** | -0.9271 | 1.73E-03 |
| **3.35** | -0.9281 | 1.67E-03 |
| **3.40** | -0.9291 | 1.62E-03 |
| **3.45** | -0.9300 | 1.50E-03 |
| **3.50** | -0.9311 | 1.58E-03 |
| **3.55** | -0.9320 | 1.53E-03 |
| **3.60** | -0.9329 | 1.46E-03 |
| **3.65** | -0.9338 | 1.49E-03 |
| **3.70** | -0.9347 | 1.47E-03 |
| **3.75** | -0.9355 | 1.38E-03 |
| **3.80** | -0.9363 | 1.34E-03 |
| **3.85** | -0.9371 | 1.29E-03 |
| **3.90** | -0.9379 | 1.25E-03 |
| **3.95** | -0.9386 | 1.22E-03 |
| **4.00** | -0.9395 | 1.28E-03 |
| **4.05** | -0.9400 | 1.10E-03 |
| **4.10** | -0.9409 | 1.22E-03 |
| **4.15** | -0.9415 | 1.13E-03 |
| **4.20** | -0.9422 | 1.17E-03 |
| **4.25** | -0.9429 | 1.12E-03 |
| **4.30** | -0.9435 | 1.06E-03 |
| **4.35** | -0.9442 | 1.08E-03 |
| **4.40** | -0.9447 | 1.02E-03 |
| **4.45** | -0.9454 | 1.04E-03 |
| **4.50** | -0.9459 | 9.70E-04 |
| **4.55** | -0.9465 | 9.99E-04 |
| **4.60** | -0.9471 | 9.56E-04 |
| **4.65** | -0.9477 | 9.61E-04 |
| **4.70** | -0.9483 | 9.90E-04 |
| **4.75** | -0.9488 | 9.68E-04 |
| **4.80** | -0.9493 | 9.76E-04 |
| **4.85** | -0.9500 | 1.10E-03 |
| **4.90** | -0.9505 | 1.11E-03 |
| **4.95** | -0.9508 | 9.16E-04 |
| **5.00** | -0.9513 | 8.75E-04 |

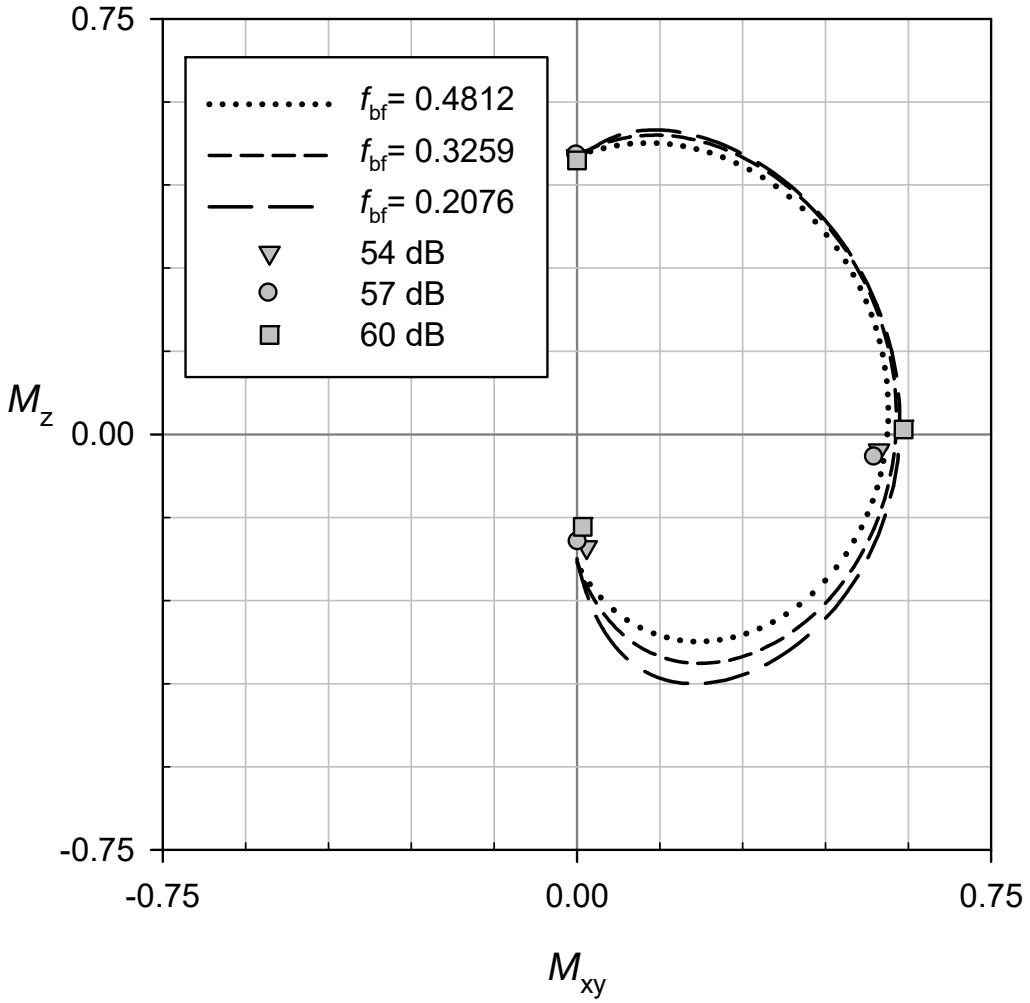


Figure 5. Calculated trajectories of net magnetization (dashed lines) and experimentally derived, normalized $M_{xy}$ and $M_z$ values at 0°, 90°, and 180° (filled symbols) during a 250-ms HS1 inversion at three different $B_1$ power levels. The resulting inversion of magnetization is identical within the margins of experimental error.

# 4. CONCLUSION

Previously, we have presented a model for predicting relaxation of magnetization during frequency-selective adiabatic pulses, requiring only knowledge of sample $T_1$ and angular motion of the effective field in the standard rotating frame. The model was successfully applied to inversion of equilibrium magnetization by low-power frequency-selective HS1 pulses. However, in certain pulse sequences (e.g., for solvent suppression), adiabatic pulses are also applied to net magnetizations that are not fully recovered to thermodynamic equilibrium. Therefore, the validity of the model was expanded to predict relaxation when HS1 pulses are applied to incompletely recovered net magnetizations. A linear relationship was found between magnetization before and after the HS1 inversion. In addition, an HS1 pulse will completely saturate magnetization in the frequency-selected range if the magnetization before the pulse is below a threshold value that is given by the pulse width and sample relaxation time. The model also accounts for changes in $B_1$ power level, which may alter the trajectory of magnetization during the HS1 pulse but not the final magnetization after inversion. The model presented here is especially amenable to convenient optimization of sequences in which HS1 pulses are employed. Future investigations will utilize the model to enhance performance of solvent suppression sequences, such as the newly developed presaturation sequence EXCEPT.

# REFERENCES


1. Garwood M, Uğurbil K. $B_1$ Insensitive Adiabatic RF Pulses. 1992:109-47.

2. Michaeli S, Sorce DJ, Idiyatullin D, Ugurbil K, Garwood M. Transverse relaxation in the rotating frame induced by chemical exchange. J Magn Reson. 2004;169(2):293-9.

3. Sorce DJ, Michaeli S, Garwood M. Relaxation during adiabatic radiofrequency pulses. Current Analytical Chemistry. 2007;3(3):239-51.

4. Mangia S, Liimatainen T, Garwood M, Michaeli S. Rotating frame relaxation during adiabatic pulses vs. conventional spin lock: simulations and experimental results at 4 T. Magn Reson Imaging. 2009;27(8):1074-87.

5. Pfaff AR, McKee CE, Woelk K. Predicting the effect of relaxation during frequency-selective adiabatic pulses. Journal of Magnetic Resonance. 2017.

6. Tannus A, Garwood M. Adiabatic pulses. NMR Biomed. 1997;10(8):423-34.

7. Garwood M, DelaBarre L. The return of the frequency sweep: designing adiabatic pulses for contemporary NMR. J Magn Reson. 2001;153(2):155-77.

8. Satterfield ET, Pfaff AR, Zhang W, Chi L, Gerald RE, 2nd, Woelk K. EXponentially Converging Eradication Pulse Train (EXCEPT) for solvent-signal suppression in investigations with variable T1 times. J Magn Reson. 2016;268:68-72.

9. Mani S, Pauly J, Conolly S, Meyer C, Nishimura D. Background suppression with multiple inversion recovery nulling: Applications to projective angiography. Magnet Reson Med. 1997;37(6):898-905.

10. Dixon WT, Sardashti M, Castillo M, Stomp GP. Multiple inversion recovery reduces static tissue signal in angiograms. Magnet Reson Med. 1991;18(2):257-68.

11. Silver MS, Joseph RI, Hoult DI. Highly selective and π pulse generation. Journal of Magnetic Resonance (1969). 1984;59(2):347-51.

12. Bro R, De Jong S. A fast non-negativity-constrained least squares algorithm. Journal of Chemometrics. 1997;11(5):393-401.

13. De Graaf RA, Luo Y, Garwood M, Nicolay K. B1-Insensitive, Single-Shot Localization and Water Suppression. Journal of Magnetic Resonance, Series B. 1996;113(1):35-45.

14. De Graaf RA, Nicolay K. Adiabatic water suppression using frequency selective excitation. Magnet Reson Med. 1998;40(5):690-6.

15. Tesiram YA, Separovic F. Matrix method for analysis of selective NMR pulses. Concepts in Magnetic Resonance Part A. 2005;25A(1):1-17.

16. Bloch F. Generalized Theory of Relaxation. Physical Review. 1957;105(4):1206-22.

# SECTION

# 2. CONCLUSION

$^1$H NMR investigations of biomolecules in their natural environment or reaction intermediates and products that are yielded in non-deuterated water as the solvent usually necessitate solvent-suppression pulse sequences to avoid interference from the overwhelming water signal. However, implementation of solvent-suppression sequences may not be straightforward, and variations that affect the sample's longitudinal and transverse relaxation times or the $B_1$ homogeneity around the sample may warrant frequent readjustment of the sequence to achieve acceptable suppression results. To address this issue, a new solvent suppression sequence, named EXCEPT for "EXponentially Converging Eradication Pulse Train", was developed. This sequence offers user-friendly, reliable suppression of solvent signals even when confronted with samples exhibiting widely different $T_1$ relaxation times or susceptibilities.

Discrepancies between computer-simulated and experimental EXCEPT performance prompted investigations of relaxation during the frequency-selective, adiabatic hyperbolic secant pulse (HS1) upon which the EXCEPT sequence depends for successful inversion-recovery nulling. It was discovered that relaxation during frequency-selective HS1 pulses is indeed significant, and a numerical computer model for predicting angular motion and magnitude of net magnetization using standard $T_1$ and $T_2$ relaxation times was developed. The model differs from existing reports of relaxation during non-frequency-selective adiabatic broad-band pulses, wherein dipolar relaxation and sometimes relaxation based on chemical exchange dominate. In a further study, the new

predictive model was tested for applications in which the magnetization before the adiabatic pulse is not at thermodynamic equilibrium. The investigations revealed a linear relationship between the initial net magnetization before and the final magnetization after an adiabatic HS1 inversion. This linear relationship provides for a simple and effective tool for the optimization of NMR sequences in which frequency-selective adiabatic HS1 pulses are used.

In future work, the innovations presented in this work will be utilized for second-generation EXCEPT sequences, in which the interpulse delays are independently computer-optimized for minimum residual solvent magnetization. The predictive power of the model may also be extended to other types of frequency-selective adiabatic pulses such as $HS^n$ and CHIRP.(1, 2) In addition, three-dimensional localization of magnetization using the RIDE ‘n RIPT sequence (3) may be undertaken to obtain a more detailed picture of magnetization trajectories and relaxation effects during adiabatic rotations. While the model described in “Predicting the effect of relaxation during frequency-selective adiabatic pulses” and “A fast and simple way to predict relaxation during a frequency-selective adiabatic hyperbolic secant pulse (HS1 sech pulse)” provides a reasonably close approximation that is useful for most NMR applications, the source(s) of some remaining discrepancies between experimental and simulated final net magnetization should also be investigated.

# REFERENCES


1. Zhang W. NMR investigations of biomass-to-fuel conversions by hydrothermal processes: Missouri University of Science and Technology; 2010.

2. Zhao H, Holladay JE, Brown H, Zhang ZC. Metal chlorides in ionic liquid solvents convert sugars to 5-hydroxymethylfurfural. Science. 2007;316(5831):1597-600.

3. Roman-Leshkov Y, Barrett CJ, Liu ZY, Dumesic JA. Production of dimethylfuran for liquid fuels from biomass-derived carbohydrates. Nature. 2007;447(7147):982-5.

4. McKay RT. Chapter 2 Recent Advances in Solvent Suppression for Solution NMR: A Practical Reference. Annual Reports on NMR Spectroscopy. 66: Academic Press; 2009. p. 33-76.

5. Hore PJ. Solvent suppression. 1989;176:64-77.

6. Guéron M, Plateau P. Water Signal Suppression in NMR of Biomolecules. 2007.

7. Price WS. Water Signal Suppression in NMR Spectroscopy. 1999;38:289-354.

8. Piotto M, Saudek V, Sklenář V. Gradient-tailored excitation for single-quantum NMR spectroscopy of aqueous solutions. Journal of Biomolecular NMR. 1992;2(6):661-5.

9. Ogg RJ, Kingsley RB, Taylor JS. WET, a T1- and B1-Insensitive Water-Suppression Method for in Vivo Localized 1H NMR Spectroscopy. Journal of Magnetic Resonance, Series B. 1994;104(1):1-10.

10. Garwood M, Uğurbil K. $B_1$ Insensitive Adiabatic RF Pulses. 1992:109-47.

11. Kato T. On the Adiabatic Theorem of Quantum Mechanics. Journal of the Physical Society of Japan. 1950;5(6):435-9.

12. Tannus A, Garwood M. Adiabatic pulses. NMR Biomed. 1997;10(8):423-34.

13. Garwood M, DelaBarre L. The return of the frequency sweep: designing adiabatic pulses for contemporary NMR. J Magn Reson. 2001;153(2):155-77.

14. Sorce DJ, Michaeli S, Garwood M. Relaxation during adiabatic radiofrequency pulses. Current Analytical Chemistry. 2007;3(3):239-51.

15. Mangia S, Liimatainen T, Garwood M, Michaeli S. Rotating frame relaxation during adiabatic pulses vs. conventional spin lock: simulations and experimental results at 4 T. Magn Reson Imaging. 2009;27(8):1074-87.

16. Michaeli S, Grohn H, Grohn O, Sorce DJ, Kauppinen R, Springer CS, Jr., et al. Exchange-influenced T2rho contrast in human brain images measured with adiabatic radio frequency pulses. Magn Reson Med. 2005;53(4):823-9.

17. Michaeli S, Sorce DJ, Idiyatullin D, Ugurbil K, Garwood M. Transverse relaxation in the rotating frame induced by chemical exchange. J Magn Reson. 2004;169(2):293-9.

18. Bohlen JM, Bodenhausen G. Experimental Aspects of Chirp NMR Spectroscopy. Journal of Magnetic Resonance, Series A. 1993;102(3):293-301.

19. Tannús A, Garwood M. Improved Performance of Frequency-Swept Pulses Using Offset-Independent Adiabaticity. Journal of Magnetic Resonance, Series A. 1996;120(1):133-7.

20. Woelk K, Trautner P, Niessen HG, Gerald Ii RE. RIDE'n RIPT—ring down elimination in rapid imaging pulse trains. Journal of Magnetic Resonance. 2002;159(2):207-12.

# VITA

Annalise Rose Pfaff was born in St. Louis, Missouri on February 5, 1989. She attended St. Pius X High School in Festus, Missouri, and enrolled at Missouri University of Science and Technology in 2007. She joined Dr. Klaus Woelk's research group as a freshman, and completed two OUREs (Opportunities for Undergraduate Research) projects with his research group. She graduated *summa cum laude* 2011 with a Bachelor of Arts in Chemistry with Secondary Education Emphasis Area.

Performing scientific research as an undergraduate inspired her to continue her education as a PhD student in the Department of Chemistry at Missouri S&T. She completed an M.S. without thesis in 2014. In addition to NMR and biochemistry research, her secondary education background and experience as a LEAD PLA for General Chemistry motivated her to take a leadership role in the General Chemistry Laboratory course redesign in Fall 2015 and Fall 2016. She earned a PhD in Chemistry in December 2017.